AD-A106 972 COLD REGIONS RESEARCH AND ENGINEERING LAB HANOVER NH F/G 19/3
PROCEEDINGS OF THE INTERNATIONAL SOCIETY FOR TERRAIN-VEHICLE SY--ETC(U)
JUL 81 W L HARRISON

UNCLASSIFIED CRREL-SR-81-16 NL

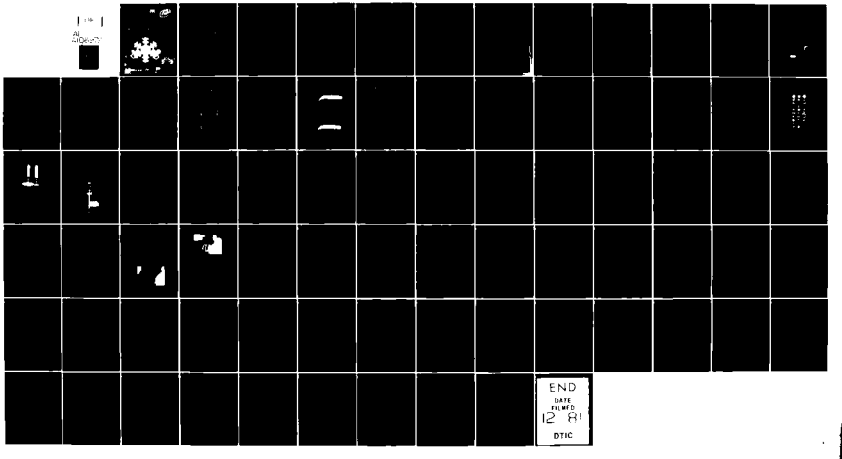

LEVEL II

Special Report 81-16

July 1981

AD A106972

PROCEEDINGS OF THE INTERNATIONAL SOCIETY FOR TERRAIN-VEHICLE SYSTEMS WORKSHOP ON SNOW TRACTION MECHANICS

Alta, Utah, 29 January-2 February 1979

W.L. Harrison, Editor

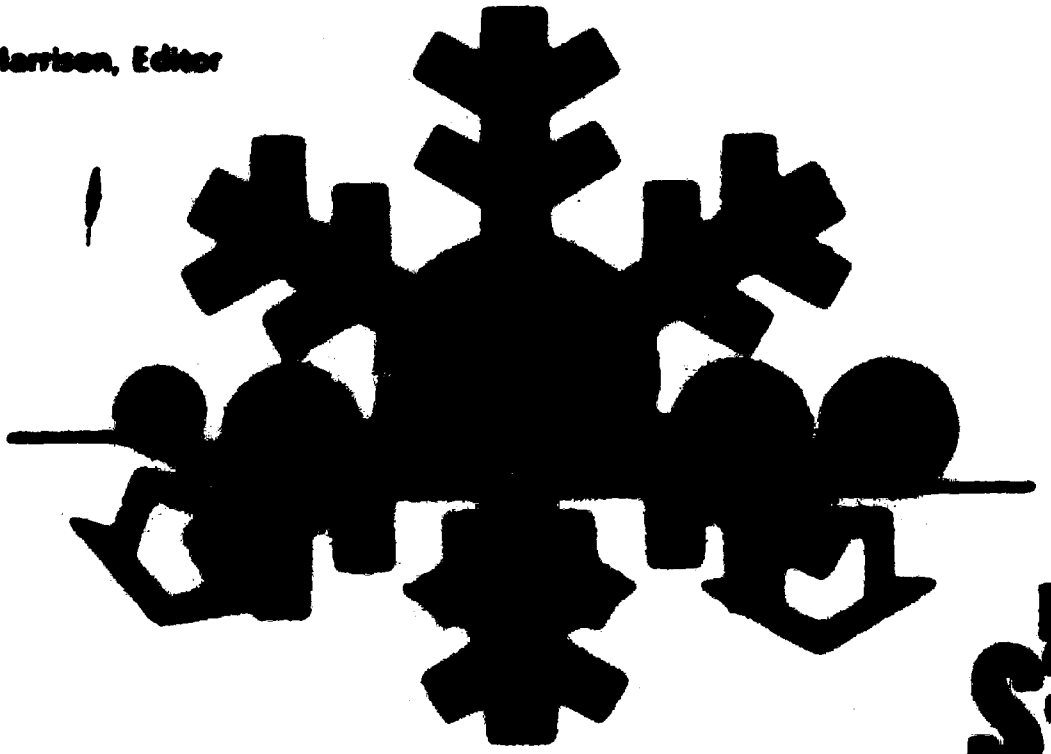

Unclassified
SECURITY CLASSIFICATION OF THIS PAGE (When Data Entered)

REPORT DOCUMENTATION PAGE	READ INSTRUCTIONS BEFORE COMPLETING FORM
1 REPORT NUMBER: Special Report 81-16	2 GOVT ACCESSION NO. / 3 RECIPIENT'S CATALOG NUMBER
4 TITLE (and Subtitle): PROCEEDINGS OF THE INTERNATIONAL SOCIETY FOR TERRAIN-VEHICLE SYSTEMS WORKSHOP ON SNOW TRACTION MECHANICS, ALTA, UTAH, 29 JANUARY-2 FEBRUARY 1979	5 TYPE OF REPORT & PERIOD COVERED / 6 PERFORMING ORG REPORT NUMBER
7 AUTHOR(s): William L. Harrison, Editor	8 CONTRACT OR GRANT NUMBER(s)
9 PERFORMING ORGANIZATION NAME AND ADDRESS: U.S. Army Cold Regions Research and Engineering Laboratory, Hanover, New Hampshire 03755	10 PROGRAM ELEMENT PROJECT TASK AREA & WORK UNIT NUMBERS
11 CONTROLLING OFFICE NAME AND ADDRESS: U.S. Army Cold Regions Research and Engineering Laboratory, Hanover, New Hampshire 03755	12 REPORT DATE: July 1981 / 13 NUMBER OF PAGES: 11
14 MONITORING AGENCY NAME & ADDRESS (if different from Controlling Office): 14 CRREL-SR-81-16	15 SECURITY CLASS (of this report): Unclassified / 15a DECLASSIFICATION/DOWNGRADING SCHEDULE

16 DISTRIBUTION STATEMENT (of this Report)

Approved for public release; distribution unlimited.

17 DISTRIBUTION STATEMENT (of the abstract entered in Block 20, if different from Report)

18 SUPPLEMENTARY NOTES

19 KEY WORDS (Continue on reverse side if necessary and identify by block number)

Mathematical predictors
Snow
Tracked vehicles
Traction
Trafficability
Wheels

20 ABSTRACT (Continue on reverse side if necessary and identify by block number)

This report reviews the state of the art of snow traction mechanics and presents the results of a limited field exercise that allowed participants to observe and practice current snow measurement processes and vehicle test procedures. The prime recommendations of the workshop attendees were 1) the use of parameters basic to the laws of physics for the classification of snow strength, and 2) the use of instrumented tracked and wheeled vehicles for snow strength measurements.

DD FORM 1 JAN 73 1473 EDITION OF 1 NOV 65 IS OBSOLETE

Unclassified 037200
SECURITY CLASSIFICATION OF THIS PAGE (When Data Entered)

PREFACE

The International Society for Terrain-Vehicle Systems (ISTVS) workshop on Snow Traction Mechanics was held at Alta, Utah, 29 January through 2 February 1979. The workshop was jointly sponsored by the ISTVS, the Geotechnical Research Centre of McGill University, and the U.S. Army Cold Regions Research and Engineering Laboratory, Hanover, New Hampshire. The workshop was to seek a mathematical identity for snow and a method of predicting snow response behavior.

The ISTVS Committee on Snow, which was responsible for the organization of the workshop, wishes to acknowledge the valuable contributions and support provided by:

Alta Ski Lifts Corp.
Bombardier Co., Ltd.
Nevada Automotive Test Center
Thiokol, Inc., Tracked Vehicle Division

The committee also wishes to acknowledge the assistance of Rosemarie Alexander who served as workshop coordinator and the hospitality of Jim and Alfreda Shane of the Goldminer's Daughter Lodge.

CONTENTS

ILLUSTRATIONS

LIST OF PARTICIPANTS

Hans Akesson
Suckarnas Alle 9
63239 Eskilstuns
Sweden
(Volvo BM)

A.W. Altum
Alta Ski Lifts
Alta, Utah 84070

Jerry Arnold
P.O. Box 234
Carson City, Nevada 89701
(Nevada Automotive Test Center

C.L. Barnett
P.O. Box 234
Carson City, Nevada 89701
(Nevada Automobile Test Center)

Mike Beeley
1067 Sumac
Logan, Utah 84321
(Thiokol)

Roger Berger
U.S. Army CRREL
Hanover, New Hampshire 03755

Robert L. Brown
U.S. Army CRREL
Hanover, New Hampshire 03755
(also Montana State University
Bozeman, Montana)

M. Peter Bühler
Im Berg
CH 8330 Pfaffikon
Zurich, Switzerland
(Rolba-Ratrac A.G.)

Jim Carey
Alta Ski Lifts
Alta, Utah 84070

Tibor F. Czako
1035 Roslyn
Grosse Pte. Woods, Michigan 48236
(TARADCOM)

Leonard Della-Moretta
1796 Russell Place
Pomona, California 91767
(U.S. Forest Service)

Russ J. Ewert
Foremost Int'l. Industries
1616 Meridian Rd. N.E.
Calgary, Alberta, Canada T2A 2P1

Jim Ferrara
Box 407
Logan, Utah 84321
(Thiokol)

William L. Harrison
U.S. Army CRREL
Hanover, New Hampshire 03755

Gordon Hine
1144 Lamplighter Dr.
Logan, Utah 84321
(Thiokol)

Henry C. Hodges, Sr.
P.O. Box 234
Carson City, Nevada 89701
(Nevada Automobile Test Center)

Henry C. Hodges, Jr.
P.O. Box 234
Carson City, Nevada 89701
(Nevada Automobile Test Center)

Gerald J. Irwin
National Defence Headquarters
Ottawa, Ontario, Canada KIA 024

David L. Jones
753 Santa Clara Ave.
Claremont, CA 91711
(U.S. Forest Service)

Irmin O. Kamm
12 Barney Rd.
Towacc, New Jersey 07082
(Stevens Institute)

Carver Kennedy
254 N. 9th E.
Brigham City, Utah
(Thiokol)

Ted Knowles
6600 E. Jefferson
Detroit, Michigan 48232
(Uniroyal Tire)

Kevin Koch
1405 Camille Dr.
Carson City, Nevada 89701
(Nevada Automobile Test Center)

Werner Köeppel
6 Frankfurt/M
AM Roemerhof 35
Germany
(Battelle-Institut E.V.)

Y. Lafortune
800 Dorchester West
Montreal, Quebec, Canada
(Bombardier)

Normand Lessard
979 Montcalm
Valcourt, Quebec, Canada
(Bombardier)

Robert L. Marlowe
598 Treeside Drive
Akron, Ohio 44313
(B.F. Goodrich)

Ken Murata
21 Glen Park Drive
Ottawa, Ontario, Canada
(Department of National Defence)

James W. O'Neal
1144 E. Market St.
Akron, Ohio 44316
(Goodyear Tire & Rubber)

R.T. Preston
4 Brinton Ave.
Nepean, Ontario, Canada
(Department of National Defence)

LeRoy Pummill
P.O. Box 234
Carson City, Nevada 89701
(Nevada Automobile Test Center)

Magnus Rönnmark
Gislaved AB
S-33200 Gislaved, Sweden

Jan Scholander
Ashemsvägen 2
77600 Hedemora
Sweden
(School of Forestry, Swedish Univ.)

Bob Shane
581 N. 1100E
Bountiful, Utah 84010

W.B. Straub
1200 Firestone Parkway
Akron, Ohio 44317
(Firestone Tire & Rubber)

Raymond Yong
Geotechnical Research Center
McGill University
817 Sherbrooke St. West
Montreal, Quebec, Canada H3A 2K6
(McGill University)

PROCEEDINGS OF THE INTERNATIONAL SOCIETY FOR TERRAIN-VEHICLE

SYSTEMS WORKSHOP ON SNOW TRACTION MECHANICS

Alta, Utah, 29 January-2 February 1979

W.L. Harrison, Editor

INTRODUCTION

The workshop on Snow Traction Mechanics was held at Alta, Utah, in January 1979. The purpose of the workshop was to bring together engineers interested in the problems associated with over-snow trafficability. The attendees included engineers from the military, universities, and government agencies and from the automotive industry, tire industry, and other private corporations.

Interest among the attendees could be divided into two areas - tracked vehicles and wheeled vehicles. While these traction elements may appear to be radically different from each other, the mechanics of tire/wheel-snow and track-snow interaction are basically similar so that addressing both topics in one workshop is warranted. The problem of over-snow trafficability can also be divided into two different categories - determination of tractive capability and evaluation of power requirements in a snowpack. Both problems are relevant to the overall problem of oversnow mobility. For instance, the efficiency of a vehicle may be characterized in terms of the power utilized in deforming the snowpack. This measure could be used to design more efficient track geometry and to determine the vehicle's power requirements. Determining tractive capability is equally as important, and in some respects is more difficult. The development of ways to predict drawbar pull and gradability is important equally for tracks and wheels, and the development of good predictive methods will be of much use for design purposes.

The workshop was held over four days. To best demonstrate the problems associated with traction mechanics and to actively involve the participants in the workshop, field demonstrations were included in the program. In this way, an on-site evaluation of current methods of predicting vehicle performance could be made.

The first day of the workshop was devoted to presentation of papers by four invited speakers. These papers are presented in the order that they were given in the workshop. The topics covered traction mechanics, energetics, in-situ measurement of snow properties, and current methods of predicting vehicle performance in snow. The second and third days were devoted to the field studies. The first day of field activities involved tracked vehicles, the next day involved wheeled vehicles on shallow snow, and the last day was devoted to evaluating the field results and the current predictive methods. The participants assembled into three groups, which separately considered questions relating to vehicle trafficability and current problems. These findings were aired in the final session on the last day.

These proceedings follow the same general order of events as the actual workshop. The sponsors feel that this publication brings together for the first time a general evaluation of the over-snow vehicle performance problem, current and new methods of analysis, remaining unsolved problems, and an objective evaluation of current techniques.

SNOW TRACTION MECHANICS

by

Raymond N. Yong[1]

To understand the elements of mobility of vehicles travelling in snow-covered terrain, it is necessary to distinguish between vehicle-soil and vehicle-snow interaction mechanics. Because the rheologic performance of snow is considerably different from that of soils, and because the properties of snow are affected more by local environmental and climatic conditions than are those of soils, it is erroneous to expect models of vehicle-soil interaction to correctly describe vehicle-snow interaction. The complications arising in the consideration of vehicle mobility in snow require particular attention to the following factors:

1. Different and specific requirements for snow performance due not only to the type of vehicular loading but also to the mechanism of loading of the snow - i.e. the difference in boundary conditions between a deep snowpack and a shallow snow layer.
2. Metamorphism of snow which causes large changes in the strength and structural characteristics of the snowpack.
3. Irreversible changes in the snow structure due to vehicular loading.
4. Mechanisms of energy transfer between the vehicle running gear and the snow that affect the development of traction and production of useful work.

The significant point is that the high degree of compressibility and the structural characteristics of snow will result in a large volume change when the snow is first loaded. This volume change becomes evident as a surface compaction. Following the first pass of the vehicle, each additional pass over the same terrain will be progressively easier since the vehicle will encounter a more compact material. Resistance to motion will

---

[1] William Scott Professor of Civil Engineering and Applied Mechanics; and Director, Geotechnical Research Centre, McGill University, Montreal, Canada.

decrease and mobility will increase. In essence, the first pass in snow is the worst pass - except in dry, aged snow layers having considerable depth hoar. In contrast, in soft soils, the first pass is generally the easiest. Thus, any comparison between snow-vehicle mechanics and soil-vehicle mechanics is rather tenuous and to use one methodology to predict results in the other surface material is out of context, even for gross approximations.

Traction Mechanics in Snow

Figures 1 and 2 show the interaction between a contact element, of either a tyre or a track, and a deformable surface. Figure 1 shows a moving tyre interacting with a deformable bearing surface. Note that the elastic rebound due to the pseudo-elastic nature of the supporting terrain can be described as the difference between dynamic sinkage and rut depth. In soft soils and other kinds of inorganic or organic terrain, rebound action can occur. In soft or powder snow, by contrast, there is essentially no rebound so the interaction between the tyre and the surface can be described by a combination of compression in the substrate snow layer and shear at the snow-tyre interface.

The right-hand side of Figure 1 expresses the total energy consumed in the interaction in terms of energy dissipated at the interface due to slip shear and compaction. The application of energy balance relationships will show that for useful work to be obtained the tyre input energy must exceed the energy absorbed by dissipative mechanisms at the interface and in the substrate. The net balance is drawbar pull. If the supporting terrain consumes all the input energy, there will be no drawbar pull. This does not mean that no traction is produced. Traction describes the interaction occurring between the contacting element - in this case a tyre - with the supporting terrain material. Traction mechanics relates to the mechanisms established at the interface where an input force transfers energy to a reacting medium. If there is a surplus of input energy resulting in linear displacement, then the net traction is positive. This provides the useful work which can be measured in terms of a drawbar pull.

In Figure 2, the traction mechanics problem is examined with respect

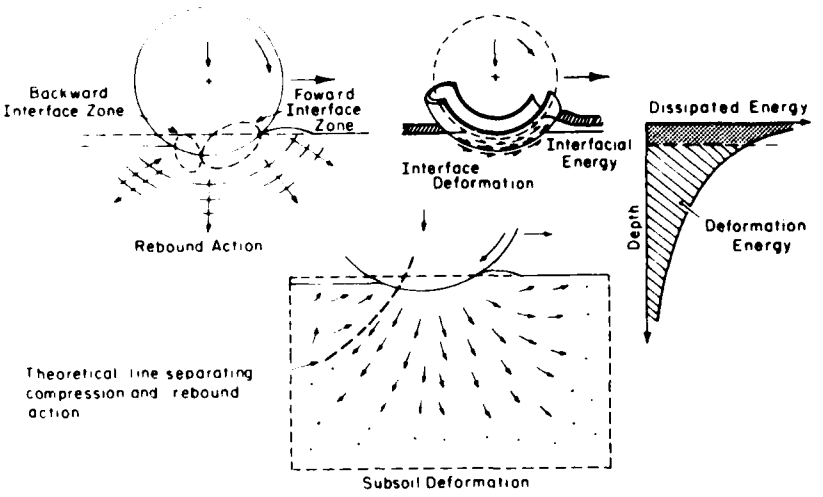

Figure 1. Substrate response and energy transfer beneath a moving rigid wheel.

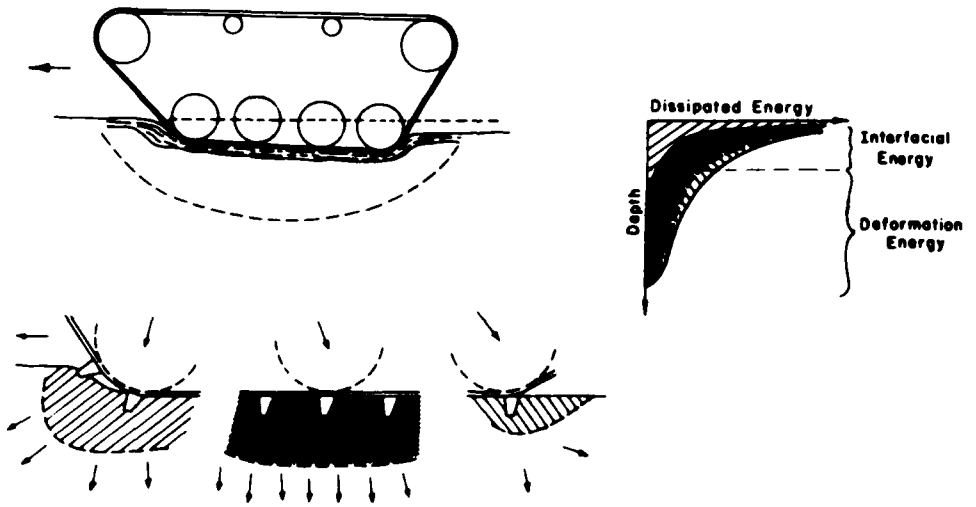

Figure 2. Substrate response and energy transfer beneath a moving track.

to a moving track on a soft terrain. In essence, as has been described previously by many other researchers, the track can be considered as an infinite radius wheel. In this particular instance, Figure 2 shows the track reacting against four road wheels. The mechanisms established bear a similarity to that shown by Figure 1 - the tyre interaction with the supporting terrain - where both slip and deformation of the substrate exist. The right-hand side of the figure shows the dissipative energy components and the total energy consumed.

We can begin to generalize the problem of interaction and explore the essentials of traction mechanics by examining Figure 3. This figure shows the running gear as a general shape and the interaction zones in the supporting material as a slip zone at and near the interface and a deformed material zone directly below the slip zone. The right side of the figure relates the energy consumed by the supporting material to resultant track motion, and input energy provided to the rate of slip caused by the interaction between the running gear and the supporting terrain material. The difference between the input energy provided by the running gear and the energy losses due to production of slip and work expended due to sinkage can be shown as drawbar pull. The efficiency of traction is defined in terms of a maximum amount of pull for a minimum input energy, or conversely the least expenditure of energy to obtain the most work. We cannot properly examine the details of the interaction at the interface to provide a better appreciation of the best system for interaction with the supporting terrain material, which provides the least energy loss.

To evaluate the elements of traction mechanics, we reduce the problem to one of track-terrain interaction in a generic form. Figure 4 shows an idealized track in motion and the resultant shear and displacements. The resistance of the supporting terrain material to the shear developed by the moving grousers controls the amount of traction that can be developed. The greater the traction resistance in the material, i.e. the greater the resistance to shear in the material, the greater the drawbar pull provided by the track. The amount of energy input (i.e. work done) that can be absorbed by the supporting terrain material without collapse, either through

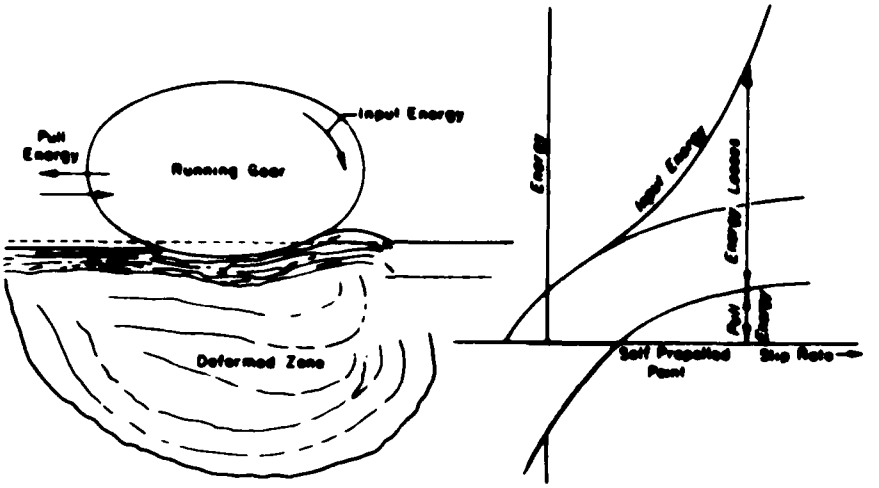

Figure 3. Energy input and dissipation in production of useful work (pull energy).

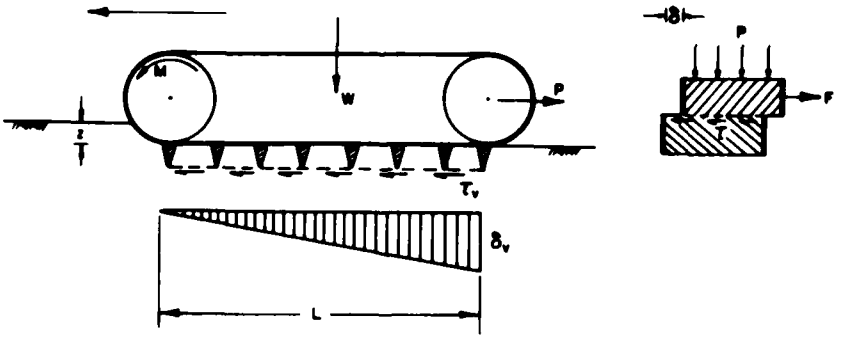

Figure 4. Idealized track motion and resultant shear.

shear, sinkage, or a combination of both, will determine the drawbar pull. With a tracked vehicle, the work exerted by the track on the supporting material without causing shear failure can be directly translated to drawbar pull. This result contrasts with that obtained for a tyre.

To illustrate the above discussion, Figure 5 shows the relative displacement of representative points in the supporting terrain material as the grousers begin to move. With continued motion, the displacement of these points can be seen by the length of the "tails" they develop. In this particular case, Figure 5 shows a flexible boundary between the two grousers. The velocities develop relative to the motion of the grousers and the displacement with time of points below and between the grousers.

By taking the forces developed and the rates of displacement, we can show (Fig. 6) how the supporting terrain dissipates the energies input by the grousers. In this figure, a rigid surface boundary connecting the grousers, which simulates a rigid track system, is compared to the flexible surface boundary, which simulates a flexible track. Note that the energy contours in the material contained between the two grousers differ markedly, depending on the type of surface boundary used. In essence, the rigid boundary dissipates less energy in the material contained between the two grousers than does the flexible boundary. In terms of efficiency, one might wish to consider this factor as significant. However, the picture is not as simple as it is presented since one must also consider the amount of energy consumed in moving a rigid or flexible track. A rigid track will generally be heavier and therefore require more energy to create motion. Thus Figure 6 is overly simplistic and only meant to convey that energy consumed in supporting terrain material is a function of the boundary conditions.

The same information given in Figure 6 can be better visualized in Figure 7. Note that the energy rate shown on the abscissa in Figure 7 essentially denotes the amount of energy consumed in the material in terms of a specific grouser displacement. The horizontal dashed line shown just below 7.5 cm indicates the slip or cutting zone phenomenon. These lines show that the influence of the original surface boundary is most marked above the slip zone contained between the grousers. Below the cutting

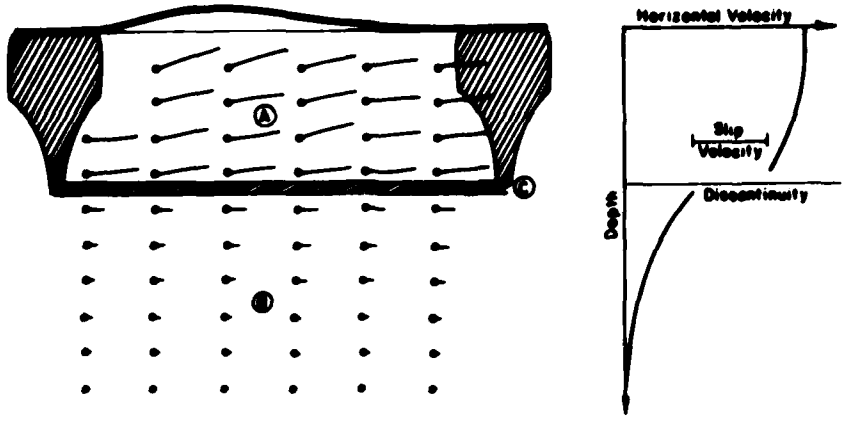

Figure 5. Relative displacement of representative points in supporting material due to grouser action.

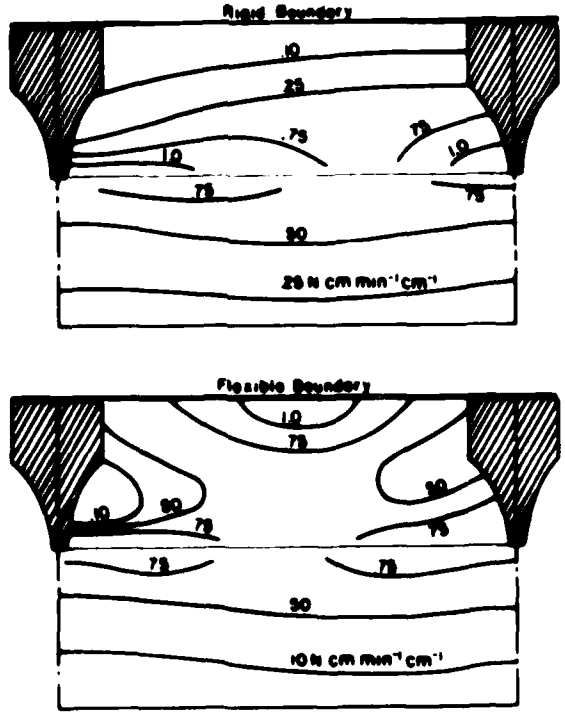

Figure 6. Energy dispersion in supporting material due to grouser action.

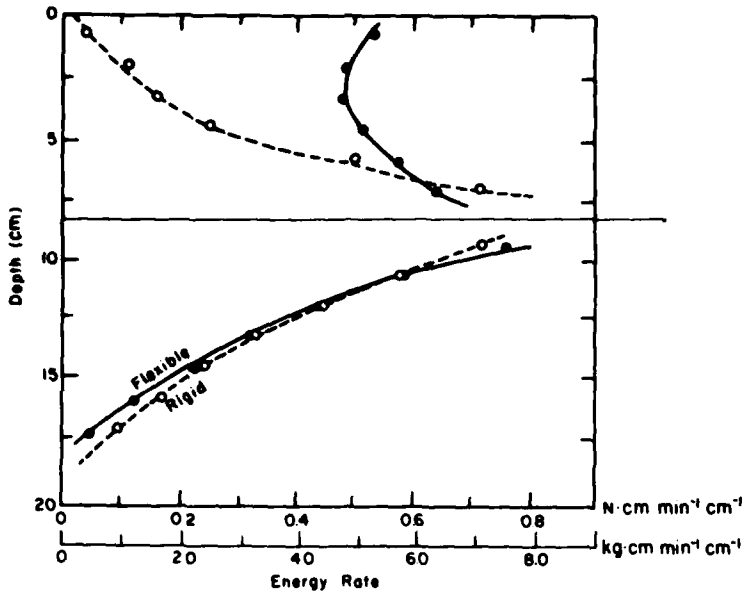

Figure 7. Energy consumed as a function of time and location.

zone, the supporting terrain is not seriously affected by boundary conditions between the grousers.

The displacement and energy rate relationships for the flexible and rigid tracks are shown in Figures 8 and 9. The two tracks have very similar maximum rates of energy consumption. However the rigid track produces the maximum consumption rate at a much lower displacement compared to the flexible track. As indicated in Figure 5, the amount of distortion energy - i.e. the energy lost in the supporting terrain material within the grousers - is less in a rigid track than in a flexible track. Figure 10 identifies how these components now relate to the overall traction developed. Figure 10 portrays zones A, B, and C. Zone A is distortion energy, Zone B is compaction energy, and Zone C is slip shear (the zone of discontinuity). By comparing Figures 8, 9, and 10, we can visualize how traction is produced in a track system and how the efficiency of the system can be improved.

Concluding Remarks

It is clear that the surface loading characteristics, which are defined by the tracks and grousers, are significant in the final production of useful work. The ability to perform useful work depends on the degree

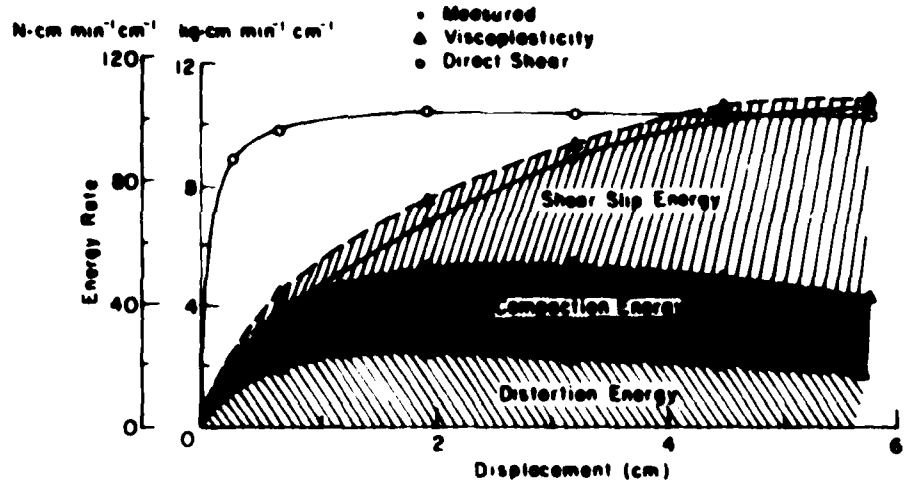

Figure 8. Displacement and energy rate relationships for flexible track.

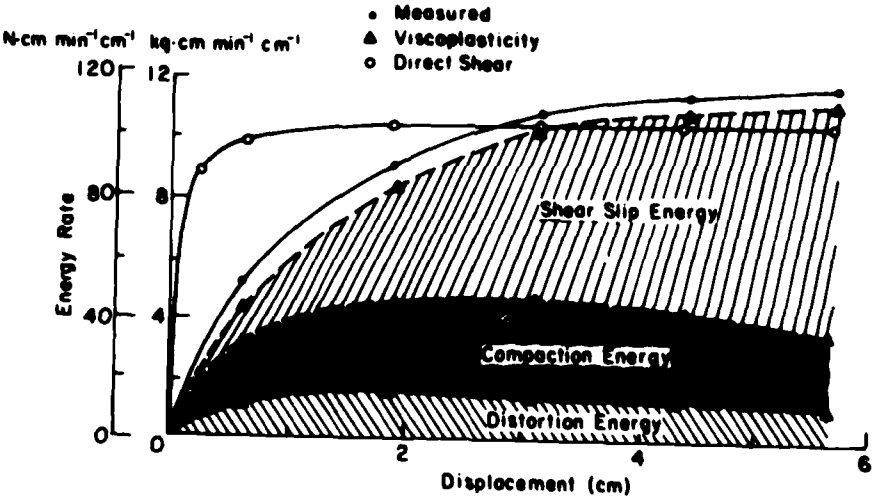

Figure 9. Displacement and energy rate relationships for rigid track.

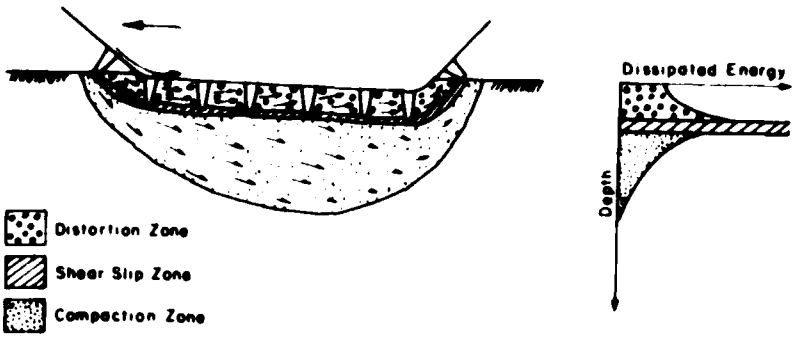

Figure 10. Traction production and energy distortion.

to which the grousers can transmit energy to the snowpack. The ability of the snow to sustain the work input without undue compaction and shear collapse will also directly influence the production of useful work. These two criteria form the basis of successful track design studies.

SNOW MEASUREMENTS IN RELATION TO VEHICLE PERFORMANCE

W.L. Harrison[2]

The purpose of this workshop in "snow-traction mechanics" is to discuss and determine the current state of the art of methods for predicting and analyzing vehicle performance over snow. The workshop will present a program that, while general in scope, will cover those aspects of snow-traction mechanics of particular interest to each participant.

We have a broad range of interests. Some of us are interested in vehicles with a high degree of agility, others in maximum traction, some with wheeled vehicles, some with tracked vehicles, and some in all facets of snow-vehicle relationships.

Snowmobiles that exert pressures of 3.0 - 6.0 kPa and travel up to 25 m/s, military tanks that exert pressures of 70 - 100 kPa and travel at 1 m/s, ski slope "grooming" vehicles with aggressive grousers (100 mm), all-wheel-drive vehicles with snow tires having 20-mm tread depth: each requires the snowpack to dissipate energy in different ways. The task at hand is to determine how the snowcover can be properly measured so that the capabilities of each type of machine and its component traction elements can be assessed.

Let us examine the current practices and attempt to agree on the snow properties that are of basic interest and useful for predicting and analyzing vehicle performance.

We must first focus on the degree of significant variation in snow properties over short periods of time. In some cases these variations can occur hourly, especially from the late winter through the spring. Daily variations are not uncommon in some areas throughout the snow season. Weekly variations can be expected in most areas. It is not uncommon to have five or six different types of snowfall over two or three days. The characteristics of any particular deposition of snow are affected by surface temperature, air temperature, wind speed, and humidity. The range

---

[2] Research Civil Engineer, Applied Research Branch, U.S. Army CRREL, Hanover, New Hampshire, U.S.A.

of possible combinations of these local environmental characteristics is obviously very, very large. This complication is more evident in shallow snow analyses than for deep snow because deep snowpacks tend to temper new deposition over a relatively short time frame, making the new layer an integral part of the composite.

With these factors somewhat in focus I shall discuss what snow property observations and measurements are made in current practice. The U.S. Army Cold Regions Research and Engineering Laboratory's "Instructions for making and recording snow observations" states the following:

"At each location (test site) the following observations should be made:

1. Snow depth (seasonal accumulation)
2. Snow surface condition
3. Snow-cover features (drifts)
4. New snow crystal type
5. Profile properties on each well defined layer
    a. thickness of layer
    b. dominant crystal or grain type
    c. density
    d. temperature
    e. hardness
    f. wetness."

An example of the results of this type of snow cover documentation is shown in Figures 11 and 12, which are classified as "deep snow" and "shallow snow" with regard to vehicle mobility.

The International Association of Hydrology publishes a report, "The International Classification for Snow," that includes all facets of the CRREL report and furthermore includes grain size, free water content, impurities, compressive yield strength, tensile strength, and shear strength at zero normal stress. The instruments to be used for measuring snow strength are not specified. Grain shape definitions are shown in Figure 13 and grain size in Figure 14.

Attention is also given to the roughness of a snow surface caused by the effects of wind, rain, melting, and evaporation. Terms and symbols are shown in Figure 15.

Data Set 21

Site 6, Border Ruffian Flat — Air temp at 1045: 4°C
ST4 & BV202 — at 1210: 2°C
23 Feb 73 — Snow depth: 121 in.
Sky: Clear — Pit depth: 48 in.

		Profile	Hardness (g/cm²) Canadian	Hardness (g/cm²) Subjective	Temperature	Density	Grain	Wetness
48 in.	6		Kb 90	Kb	−4	0.118, 0.162, 0.162 } 0.147	Fs	Wc
	6		Kb 90	Kb	−9	0.208	Fs	Wc
	6		Kb 150	Kb	−6	0.190, 0.218 } 0.204	Fs	Wa
	6		Kb 310	Kc	−6	0.242	Fs	Wa
	6		Kc 800	Kc	−5	0.278	Fs	Wa
	6		Kch 1600	Kd	−4	0.290	Fs	Wa
	6		Kcg 1200	Kd	−5	0.294	Fs	Wa
	6		Kcs 1100	Kd	−4	0.324	Fs	Wa
	73		Kd 2500	Kd	−4	0.374	Fs	Wa

Figure 11. Profile of deep snow cover (from Harrison 1975).

The penetrability of surface layers is also considered. It is determined by "a man" standing on one ski (PS) or on one foot (PP). Figure 16 shows the classification symbols for PS and PP. Figure 17 shows a reference chart for identifying snow crystal shape.

Whether these measurements and observations of snow cover characteristics are pertinent to vehicle performance over snow will be discussed later.

The cone penetrometer, the drop cone, and the ramsonde have been developed to produce indices of strength. Other devices were developed to

Data Set 10

Site 2 — Air temp: 0.5°C
M34 — Time: 1130
31 Jan 73 — Sky: Clear (clouds)

		Profile	Hardness (g/cm²) Canadian	Subjective	Temperature	Density	Grain	Wetness
9 in.	2½	New snow	Ka 30	Kb	−5.5	0.145	Fa Plates	Wc
	4½	Compacted old snow	Kch 1800	Kd	−7.0	0.434	Db	Wc
	½	Ice	6000	Ke				
	1½	Old snow	Kb 800	Kd	−6.5	0.402	Dd	Wc
	½	Ice		Ke	−7.0			

Remarks: Density in rut after 1 pass or 6 passes: 0.510.
Sample taken 2 in. below snow surface.

Figure 12. Profile of shallow snow cover.

give some quantitative values related to the compressive strength and shearing strength. Foremost and least controversial of these devices is the standard triaxial test apparatus. This device is also the most difficult to use properly and the least adapted to field use.

The Canadian hardness gauge shown in Figure 18 is generally used to establish a "hardness" profile of the snow which can be calculated in kPa given the spring rate and the disc area.

The vane cone (Fig. 19) measures a series of shear strength values at different normal loads by pressing the device into the snow until the desired vertical resistance (pressure) is reached. At this point the vane

Description	Symbol	Graphic Symbol
Class "a" Class "a" refers to freshly deposited snow composed of crystals, or parts of broken crystals. Snow which has lost its crystalline character while falling to earth, and graupel, ice pellets, and hail do not belong to this class. Class "a" snow is generally very soft.	a	
Class "b" This class refers to snow during its initial stage of settling. It has not reached the very fine grain-size condition which is generally regarded as the conclusion of the initial stage of transformation. Although it has lost a great deal of its crystalline character, some crystalline features can be observed. Class "b" snow is usually fairly soft.	b	
Class "c" When snow is transformed by melting, or melting followed by freezing, it completely loses all crystalline features and its grains become irregular and more or less rounded in form. This is Class "c" snow. It has no sparkle effect even in bright sunlight and can be readily recognized by its dull appearance. It is usually fairly soft when wet, but can be very hard when frozen. Class "c" snow may have any size of grains from very fine to very coarse.	c	
Class "d" At temperatures well below freezing and without any apparent melting, snow is transformed into Class "d" by the process of sublimation which produces irregular grains with flat facets. These facets give the snow a distinct sparkle effect in bright sunlight. In the Arctic, where temperatures are low and persistent winds accelerate the sublimation, practically all of the settled snow is Class "d" and has almost as much sparkle as a deposit of F1 crystals. Class "d" snow is usually fairly hard.	d	
Depth Hoar Depth hoar is characterized by its hollow cup-shaped crystals. These crystals are produced by a very low rate of sublimation during a long uninterrupted cold period and are most frequently found directly below a more or less impermeable crust in the lower part of the snow cover. The strength of a layer of depth hoar is very low.	e	

Figure 13. Grain shape definitions of snow.

GRAIN SIZE OF DEPOSITED SNOW

Term	Symbol	Grain Size Range
Very fine	a	less than 0.5 mm.
Fine	b	0.5 to 1.0 mm.
Medium	c	1.0 to 2.0 mm.
Coarse	d	2.0 to 4.0 mm.
Very coarse	e	greater than 4.0 mm.

Figure 14. Grain size definitions of snow.

Term	Symbol	Graphic Symbol
Smooth	a	
Wavy	b	
Concave furrows	c	
Convex furrows	d	
Random furrows	e	

Figure 15. Surface roughness of snow covers.

Term	Depth Range, cm.	Symbol
Very small	less than 0.5	a
Small	0.5 to 2	b
Medium	2 to 10	c
Deep	10 to 30	d
Very deep	greater than 30	e

Figure 16. Penetrability of snow cover.

SOLID PRECIPITATION

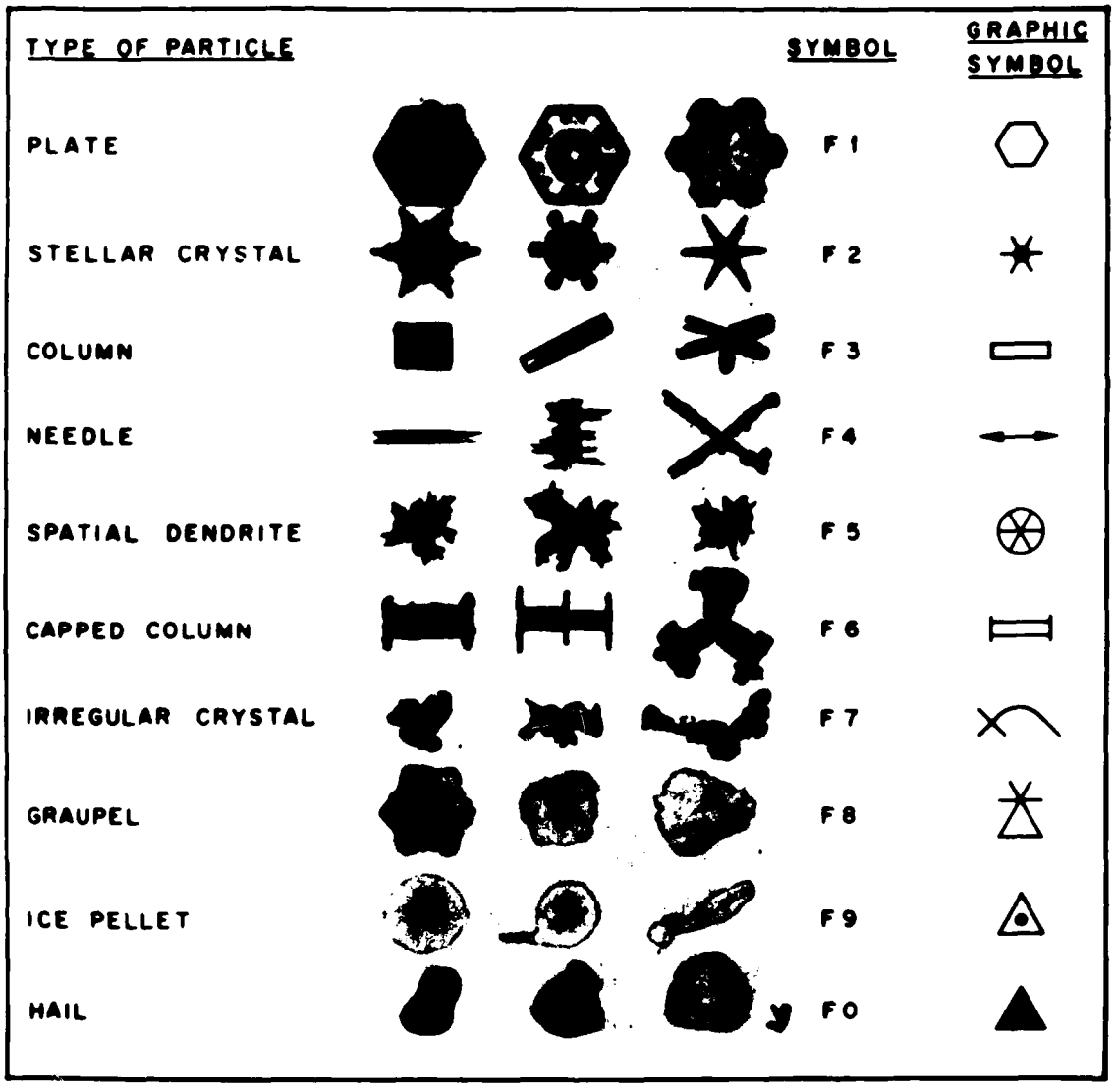

MODIFYING FEATURE	BROKEN CRYSTALS	RIME COATED CRYSTALS	CLUSTERS	WET
SYMBOL SUBSCRIPT	p	r	f	w

Figure 17. Grain shape identification.

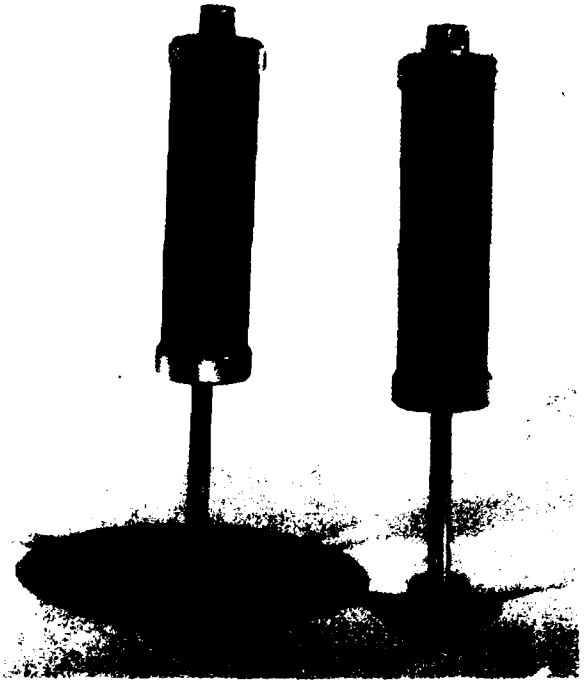

Figure 18. Canadian hardness gage.

cone is rotated. The vertical pressure is read from a proving ring and pressure gage; the resistance to shear is read directly from the torque wrench used to rotate the vane cone.

The plate sinkage test and the annular shear test are used to produce the "Bekker values" of k_c, k_ϕ, and n, along with coefficients of internal shearing resistance. When used as such, the combination of instruments is called a "bevameter."

The plate sinkage test has also been used to measure energy dissipation of snow during the compaction of shallow layers. The annulus has been used with a rubber facing in shallow and deep snow to measure the coefficients of interface shearing resistance.

The vane cone and the bevameter were demonstrated during the field exercises of the workshop. They were used along with their associated pre-

diction methodology to estimate the results of drawbar-pull demonstrations. For these reasons the measurements for each device will be discussed in more detail.

The vane-cone obtains a value f for each pressure applied. The results can be plotted as shown in Figure 20.

The equation used to determine f is

$$f = \frac{\text{vane cone torque resistance}}{\pi(\frac{d^2h}{2} + \frac{d^3}{6})} \qquad (1)$$

where d is vane diameter and h is vane height. For a given vehicle one locates the intersection of the vehicle ground pressure, p, with the curve and reads the associated value of f.

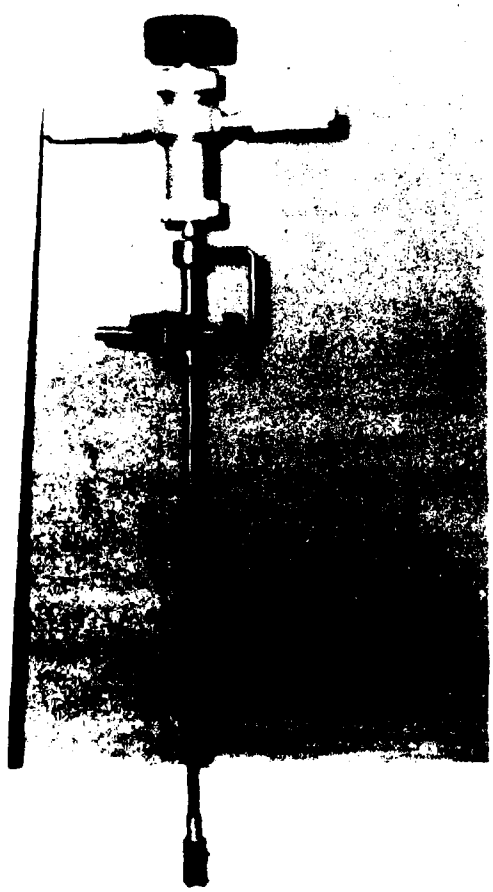

Figure 19. Vane cone apparatus.

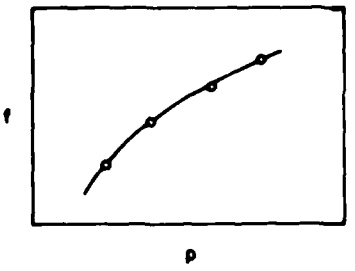

Figure 20. Graph of vane-cone results.

The plate sinkage test produces a curve as shown in Figure 21a.

The curves from Figure 21a are replotted on log-log graphs as normal pressure, p, vs. sinkage, z, in Figure 22. The intercepts of the logarithmic curves with the z=1 ordinate are designated a_1 and a_2, corresponding with the plate radii b_1 and b_2. The Bekker values of k_c, k_ϕ, and n are obtained from

$$k_\phi = \frac{a_2 b_2 - a_1 b_1}{b_2 - b_1} \qquad (2)$$

$$k_\phi = \frac{a_2 b_2 - a_1 b_1}{b_2 - b_1} \qquad (3)$$

where n is the slope of the p-z curve (log-log). The curves produced by the shear annulus are shown in Figure 22.

It is universally agreed that predicting vehicle performance requires some type of strength measurement. There is no universal agreement as to what these measurements should be or what instrument should be used to obtain them. It is hoped that in the future common strength parameters will be measured regardless of the instrument used.

In terms of documentary information, it is important that the snow cover is sufficiently described so that fellow researchers are assured of understanding the conditions and material properties in which tests were performed. Since the more the documentation, the greater the understanding, I will list what I consider the minimum information required for mobility purposes. Researchers have the option of adding as much information as time, money, and interest permit.

Density, grain size, and snow temperature profiles should be measured during the test period. The number of profiles and the times during the

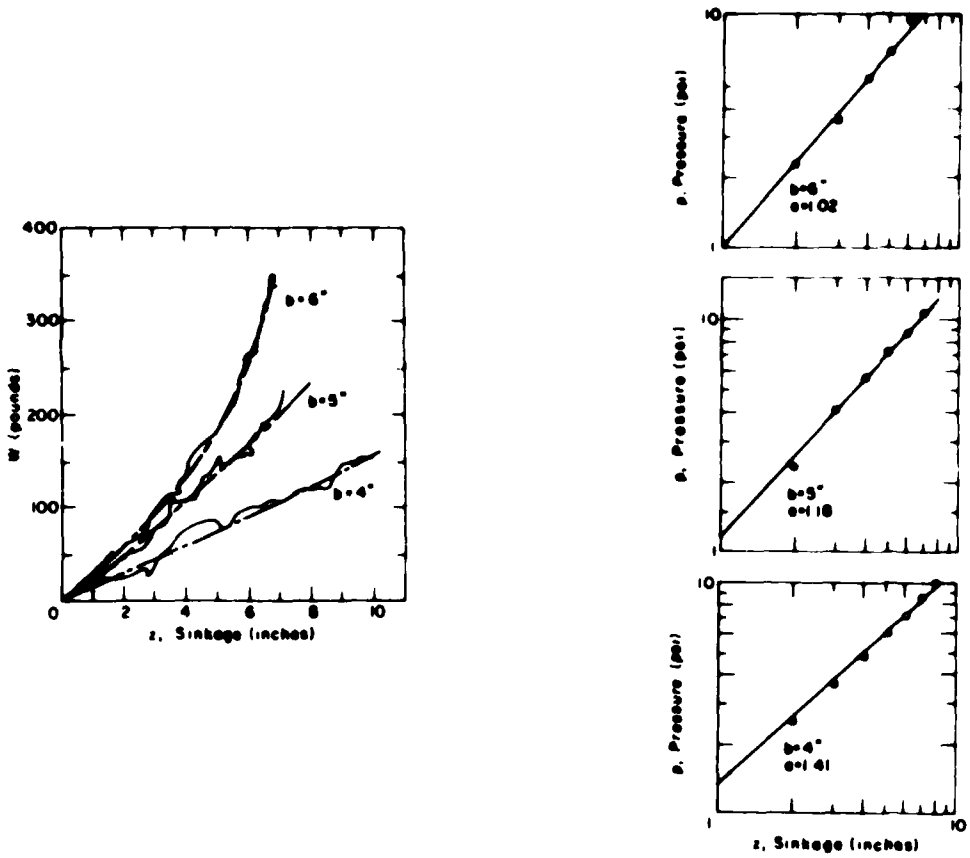

a. b.

Figure 21. Plate sinkage curves (Harrison 1957).

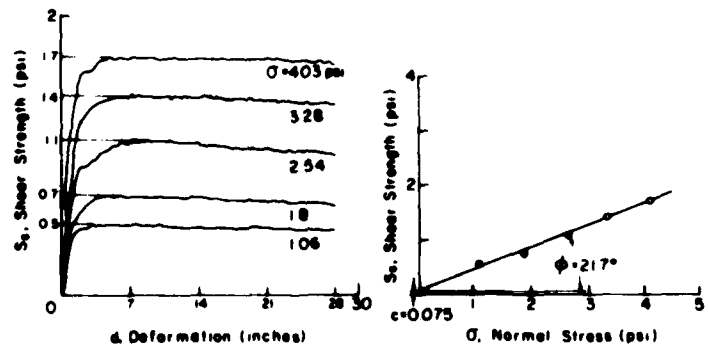

Figure 22. Shear annulus curves (Harrison 1957).

day when samples are taken is left to the discretion of the field team. This latter option is dependent on variations in the local environment during the test day. The depth of the profile should extend to at least 0.5 m below the level of disturbance in the snowpack. If this depth reaches the ground beneath the snowpack, some qualitative description of the subsurface should be recorded, i.e. whether it is frozen or unfrozen organic or mineral, pavement, etc.

Other documentary observations should be snow depth, air temperature (at least 1 m above the snow surface), and a general but brief account of local environmental conditions such as cloud cover, precipitation, and wind conditions.

These documentary data along with some sort of strength-deformation measurements will be sufficient for mobility purposes.

REFERENCES

Harrison, W.L. (1957) Study of snow values related to vehicle performance, U.S. Army Ordnance Corps, LLRB Report 23.

Harrison, W.L. (1975) Vehicle performance over snow; Mathematical model validation study. CRREL Technical Report 268.

APPLICATION OF ENERGETICS TO VEHICLE TRAFFICABILITY PROBLEMS

R.L. Brown[3]

General Discussion

This section is addressed to the problem of determining vehicle power requirements for motion in snow. As a vehicle moves through snow, considerable amounts of energy are absorbed by the snow. In many conditions, this power consumption may be a large percentage of the vehicle engine power, thereby limiting vehicle capability.

Energy consumption takes place through several mechanisms. The tracks or wheels compact the snow in the region below the track. The cross section of the compacted region of snow, termed the pressure bulb, is illustrated in Figure 23. The depth, Y_B, of the bulb may in some instances exceed a meter, depending on the vehicle track pressure, vehicle speed, track geometry, snow strength stratigraphy, and snow density stratigraphy. In cases where the vehicle is not developing appreciable slip, the energy absorbed through compaction in the pressure bulb represents the large majority of consumed energy.

Energy may also be absorbed through deviatoric deformation of the snowpack. Even in cases where there is little slip, some deviatoric deformation is present, since shear force must be exerted on the bottom of the track rut to propel the vehicle through the snow. This shear force, usually referred to as the tractical force, must induce some deviatoric deformation of the snowpack. However, the energy associated with this deformation can be shown to be small in comparison to the compactive energy if the vehicle is not pulling a heavy load such that it is approaching its traction limit. If there is slip, a good percentage of the power is expended in shear deformation in the pressure bulb and in dissipating energy along the sliding surface between the track and the track rut. Some energy is also wasted through excavation of snow in the track and disaggregation of the snow in the immediate vicinity of the tracks. This situation represents a complex combination of deformation mechanisms and would be hard to

[3] Professor, Civil Engineering Dept., Montana State University.

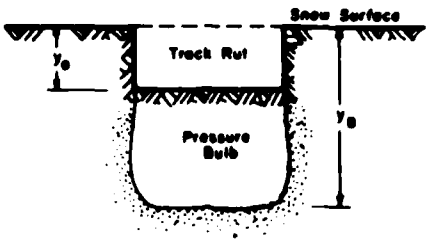

Figure 23. Geometry of track rut and pressure bulb.

describe analytically. However, the development of necessary traction appears to be the most important problem.

Since we are calculating the power absorbed in the pressure bulb and ignoring energy expenditure due to track slip, we assume the vehicle moving through the snow is not near its traction capabilities.

Figure 23 illustrates a typical pressure bulb. Y_0 and Y_B are the rut depth and the pressure bulb depth, both measured from the undisturbed snow surface. In deep snow, the pressure bulb will not extend into the ground. In this case, the bulb must be supported by the pressure along the bottom and the shear stresses along the walls. The bulb will extend downward until the pressure p is reduced to a critical value, p_c, that the snow can support without any plastic deformation. Since only small pressures are required to produce plastic compaction, p_c is generally small in comparison to the track pressure, p^*. Consequently, the pressure bulb is supported primarily by the shear stress on the bulb walls. The track pressure, p^*, is determined by the track size, vehicle weight, track geometry, the suspension system, and weight distribution of the vehicle. Usually some reasonable approximation of the track pressure can be made, although an exact description is difficult.

In shallow snow, the pressure bulb extends to the ground. The pressure bulb receives a significant amount of support from the ground, and the support from the bulb walls becomes less significant. When the track width, w, is larger than the snow depth, the effect of the shear stress on the bulb wall may be neglected without serious error.

The pressure bulb shown in Figure 23 is approximately rectangular, typical of pressure bulbs observed in the field by Harrison (1957, 1975). The bulb width is approximately equal to the track width if the vehicle is moving in a straight line and not shimmying. Usually the bulb swells about two-thirds of the way down, but this swelling does not significantly affect

the bulb's cross-sectional area. Local inhomogeneous conditions in the snowpack may alter the bulb shape, but these effects are local and will not be considered in this study.

In view of the above discussion, the pressure bulb can be idealized by the geometry shown in Figure 24. The shear stress, τ, and the critical pressure, $\hat{p}_c$, support the bulb together. Figure 24 does not show the pressure bearing in on the bulb walls and a shear stress which must exist on the bottom of the pressure bulb.

Power Requirements for Oversnow Travel

A volumetric constitutive equation is needed to calculate the energy

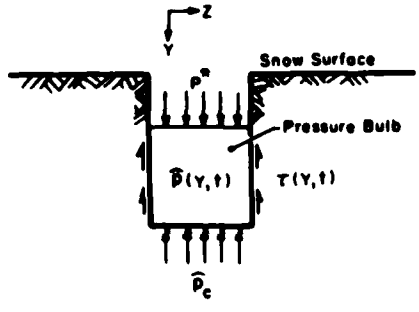

Figure 24. Idealized pressure bulb.

the snowpack absorbs as it is compacted. This can be done by relating the hydrostatic pressure, $\hat{p}$, to the density ratio, α, where

$$\alpha = \rho_m/\rho \tag{1}$$

ρ_m and ρ are the mass densities of ice and snow. The following constitutive law has been found to be representative of the volumetric behavior of snow (Brown 1979):

$$\dot{\alpha} = 0, \quad \hat{p} < \hat{p}_c$$

$$\hat{p}(t) = \frac{Je^{-\phi\alpha/\alpha_0}}{3a}\left\{2(S_o - C) + C \ln\left[\frac{(-\dot{\alpha}A)^2}{\alpha(\alpha-1)}\right]\right\}, \quad \hat{p} < \hat{p}_c \tag{2}$$

$$\hat{p}_c = \frac{J}{3\alpha_o}\left\{\ln\left(\frac{\alpha_o}{\alpha_o - 1}\right)\left[2(S_o - c) + c\ln\left(\frac{(A\alpha)^2}{\alpha_o(\alpha_o - 1)}\right)\right]\right\}e^{-\phi}$$

$\hat{p}_c$ is the critical pressure at which plastic deformation of snow begins. Both $\hat{p}$ and $\hat{p}_c$ are rate dependent. This equation has been shown to accurately represent the volumetric properties of snow for strain rates ranging from $-10^{-5}s^{-1}$ to $-20\ s^{-1}$. For such strain rates the deformation is predominantly volumetric.

Equation 2 assumes that the material is rigid until the critical pressure, $\hat{p}_c$, is reached. As pressure increases $\hat{p}$ as $\hat{p}_c$, plastic flow begins. This assumption of a rigid-viscoplastic material is quite valid for strain rates larger than $10^{-5}s^{-1}$, since the elastic strains that occur prior to the onset of inelastic deformation are infinitesimal and therefore negligible.

The critical pressure, $\hat{p}_c$, depends upon the initial density, ρ_o, and the rate of change of α. Figure 25 illustrates the variation of $\hat{p}_c$ with initial density of ρ_o. This figure is for $\dot{\alpha} = -0.1\ s^{-1}$, which is actually a fairly large strain rate, since it would produce a rate of change of density of about 20 kg $m^{-3}s^{-1}$. This is characteristic of strain rates occurring at the bottom of the pressure bulb. For pressures below the curve in Figure 25, the material does not deform plasticly, whereas for pressures above the curve, the material does deform plastically. This deformation can be calculated with eq 2.

The shear strength of snow must also be known if one is to make a stress analysis of the pressure bulb. As indicated earlier, the shear stress, τ, acting along the bulb walls supports the pressure bulb. τ acts along the bulb wall which is a failure surface, since the particles in the pressure bulb move downward while the particles outside the wall experience very little downward motion. The shear stress that can be supported at this surface depends upon the hydrostatic pressure and the relative velocity of particles on opposite sides of the wall. Following Yong and Fukue (1978) we use the relation

$$\tau = \tau_o + K\hat{p} \qquad (3)$$

τ_o and K depend on the velocity, although there are very few data available for accurately determining this relationship. τ_o has been shown by Yong and Fukue to be negligible for cases involving large pressures.

As the vehicle passes over the snowpack, the material is compressed downward in a manner similar to that shown in Figure 23. The equation of equilibrium and the equation of mass conservation can be used to describe this process mathematically. The integrated forms of these two equations are

$$\hat{p}(Y,t) = - \int_o^Y \frac{2\rho_o}{\rho_m w} \alpha \tau dy + \hat{p}(o,t) \qquad (4)$$

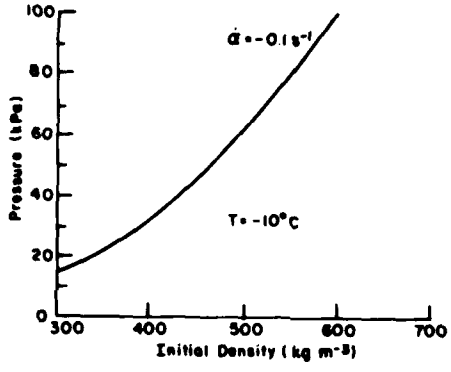

Figure 25. Variation of critical pressure with density.

$$Y_o = \int_o^{Y_B} (1 - \frac{\alpha}{\alpha_o}) \, dY \qquad (5)$$

In eq 4 $\hat{p}(Y,t)$ is the pressure inside the pressure bulb, $\hat{p}(0,t)$ is the pressure at the top of the bulb (track pressure), ρ_o is the initial snow density, and w is the track width. This equation simply requires that the pressure along the bottom of the bulb and the shear stress along the sides equal the pressure generated along the top of the bulb. In eq 5, α_o is the initial density ratio. This equation requires that the mass of the snow under the track remain constant during compaction. Y_o is the depth of the track rut.

Equation 3 can be substituted into eq 4 to eliminate the shear stress τ. Then eq 2 can be substituted into the integrand in eq 4 to eliminate $\hat{p}$. Subsequent integration of eq 4 and 5 eventually leads to calculated

values of pressure and α distributions within the pressure bulb, rut depth, and pressure bulb depth. We will give examples of these calculations later.

The next step is to calculate the energy absorbed by the snowpack due to compaction within the pressure bulb, found by calculating the work the track pressure expends while forming the rut. Consider the upper surface of the snowpack during an instant of time, dt, that the snow is being compacted. If the track pressure at this instant is $\hat{p}(0,t)$, and if during the time increment, dt, the surface is compressed downward by some distance, dy, the work done by the track pressure during this time increment is

$$dW = \hat{p}(0,t)dy(0,t) \tag{6}$$

The work rate is then

$$\frac{dW}{dt} = \hat{p}(0,t)\,\frac{dy}{dt}\,(0,t) \tag{7}$$

This term is the work rate/unit time/unit track area. Consequently the total vehicle power expended in compacting the snow is

$$P_w = \frac{A_T}{t^*}\int_o^{+*} \hat{p}(0,t)\,\frac{dy}{dt}\,(0,t)\,dt \tag{8}$$

where A_T is the area of the vehicle tracks and +* is the time that snow is under the vehicle track. This power term includes the work dissipated due to shear losses along the bulb wall and is the energy dissipated by compaction of the snow in the bulb. The term does not reflect the energy expended by track slip or by the large deviatoric deformations in the immediate vicinity of the track grousers.

Example: Tracked Vehicle With Uniform Track Pressure In Deep Snow

Idealize the track pressure according to the distribution shown in Figure 26a. The pressure is assumed to build up linearly to a constant peak track pressure, p*. This variation is given by the equation

$$\hat{p}(0,t) = p^*\,\frac{t}{t_o}\,[1 - H(t-t_o)] + p^*H(t-t_o),\ 0\leq t\leq t^* \ . \tag{9}$$

H(t) is the Heavyside step function, and t_o is the entry time, i.e. the time increment that the surface snow is in contact with the front part of the track. t_o is determined by the vehicle sinkage and speed. Figure 26b illustrates the temporal variation of $\hat{p}(0,t)$. Generally the track

pressure has a periodic variation determined by the spacing and size of the road wheels. For wheels with a moderate or small spacing, this periodic fluctuation may be neglected.

The basic track geometry and vehicle weight chosen for the calculations are those of the M5A4 high-speed tractor. This vehicle was originally designed for transporting personnel and light cargo over soft terrain. The M5A4 has a 235-horsepower gasoline engine, weighs about 12 tons, and has a track length of about 3.0 meters and a track width of 0.31 meters. The nominal track pressure varies from 43 kPa upward, depending on the load. Consequently the M5A4 cannot operate in low density seasonal snow but can operate fairly well in perennial snow, like that on the Greenland ice cap, or in medium-density seasonal snow. Such snow generally has densities in excess of 300 kg m^{-3}.

The material parameters in eq 2 are

Figure 26. Profile of track rut and pressure distribution under traffic.

$$
\begin{aligned}
J &= 3.07 \\
\phi &= 5.28 \\
S_o &= 1.0 \times 10^6 \text{ Pa} \\
C &= 1.16 \times 10^6 \text{ Pa} \\
A &= 3.3 \times 10^5 \text{ s}
\end{aligned}
\qquad (10)
$$

These properties are from the Brown (1978a) study on compressibility of snow.

Figures 27-32 summarize the results of the calculations. Only snow densities in excess of 300 kg m^{-3} were considered, since the constitutive equation, eq 2, is not considered valid for low density snow. The results are presented in terms of vehicle horsepower requirements, since this is the most recognizable unit of power. The track pressures considered were

for the most part larger than 20 kPa, since for medium-to-high density snow, the pressure bulb consumes insignificant energy at track pressures below 20 kPa.

Figures 26 and 27 demonstrate the very strong dependence of energy consumption on initial density and nominal track pressure. For instance merely increasing the pressure from 30 kPa to 90 kPa results in an order of magnitude increase in energy consumption for snow with a density of 300 kg m^{-3}. Conversely, snow with an initial density of 500 kg m^{-3} consumes only about 10% as much energy as snow with an initial density of 300 kg m^{-3} (see Fig. 28). As indicated by Brown (1978b) and by Figure 28, for a given pressure p*, a critical density exists above which very little compaction and energy consumption takes place. Figure 28 shows that for initial densities above 450 kg m^{-3} a track pressure of 60 kPa produces very little compaction.

Figure 29 demonstrates the effect of track geometry on track efficiency. The M5A4 has a length-width ratio of about 10. Figure 29 shows how energy consumption varies for a range in L/w from 2 to 10. A long narrow track has an obvious advantage partly because of how the shear stress helps support the pressure bulb. One can see from Figure 24 that the pressure bulb would have to be deeper for a wide track if the wall shear stresses were to support the bulb. An articulated vehicle with a large L/w ratio should perform well in snow and still be reasonably maneuverable.

Figure 30 shows the variation of bulb depth with track pressure for three initial snow densities. As should be expected, bulb depth decreases with decreasing pressure and with increasing density. The variation of bulb depth with track length-width ratio is illustrated in Figure 31; Figure 32 gives the vertical variation of bulb pressure for one particular case. As can be seen, the depth is dependent on the value of $\hat{p}_c$. The yield pressure is given by eq 2. Over the bottom 0.4 meter of the bulb, the pressure, $\hat{p}$, varies relatively little, so changing the critical pressure of deformation, $\hat{p}_c$, by some arbitrary amount could cause a significant change in the bulb depth. This, however, would not affect power consumption much, since most of the energy is consumed in the upper portion of the bulb where the greatest amount of compaction takes place.

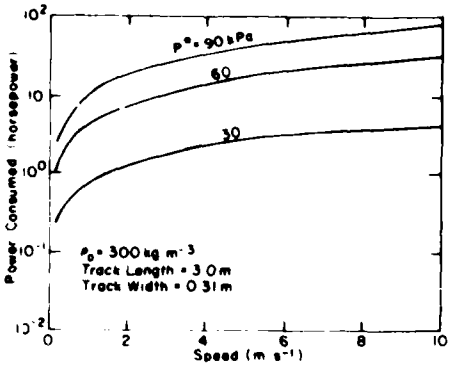

Figure 27. Variation of power absorbed in deep snowpack.

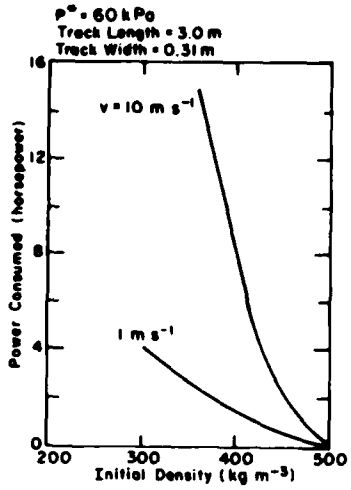

Figure 28. Power dissipated by deep snowpack as a function of initial density.

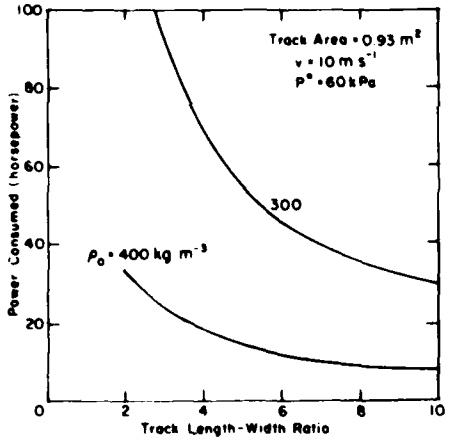

Figure 29. Effect of track geometry on power requirements in deep snowpack.

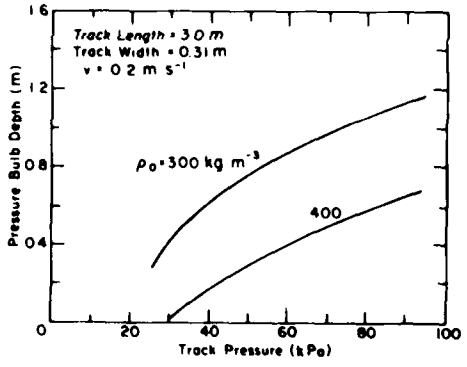

Figure 30. Variation of pressure bulb depth with nominal track pressure.

Finally, Figure 33 shows the compactive force generated by the motion of the vehicle in the snow. This was obtained by integrating the horizontal component of the track pressure over the track area. Note the improvement of track efficiency with vehicle speed.

Example: Vehicle With Uniform Track Pressure in Shallow Snow

In shallow snow, the pressure bulb is primarily supported either by the ground or by a structurally rigid layer of ice or packed snow. In this case, the contribution of the shear stress on the walls of the bulb can be neglected, and the pressure distribution under the track becomes relatively uniform. The vehicle horsepower absorbed by the snowpack can be shown to be

$$P_w = \frac{2LWH}{\alpha_o t^*} \int_o^{t^*} \beta \dot{\alpha} dt \qquad (11)$$

This solution was derived in a manner similar to the previous power calculations, but in this case the pressure distribution was assumed to be uniform in the bulb, since the shear stresses on the bulb wall were ignored. The pressure β in the bulb is therefore the same as the nominal track pressure.

Figures 34 and 35 illustrate results for a vehicle in shallow (0.25 m) snow. In this case, power consumption is considerably lower than what it would be in deep snow. Figure 34 shows the variation of power with vehicle speed; Figure 35 shows the effect of initial density on power consumption.

Some Concluding Remarks

The problem of vehicle power expenditure in snow is a complicated

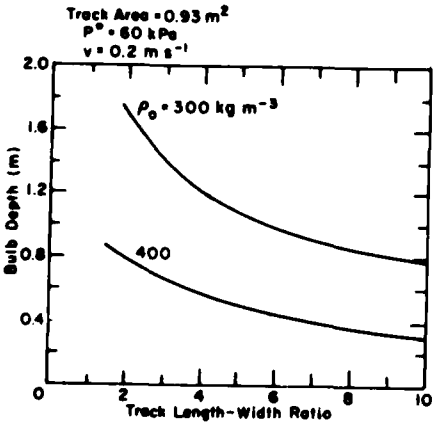

Figure 31. Effect of track geometry on bulb depth.

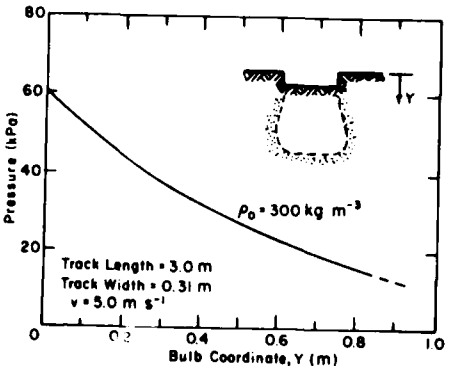

Figure 32. Pressure distribution inside pressure bulb in deep snowpack.

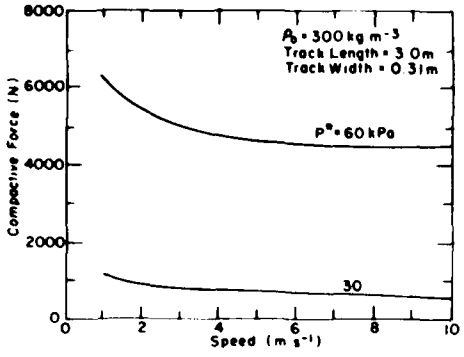

Figure 33. Variation of compactive force with vehicle speed.

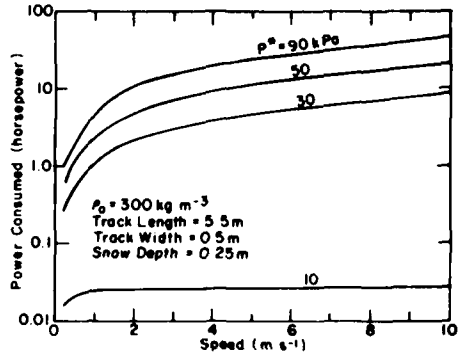

Figure 34. Power consumption in shallow snowpack.

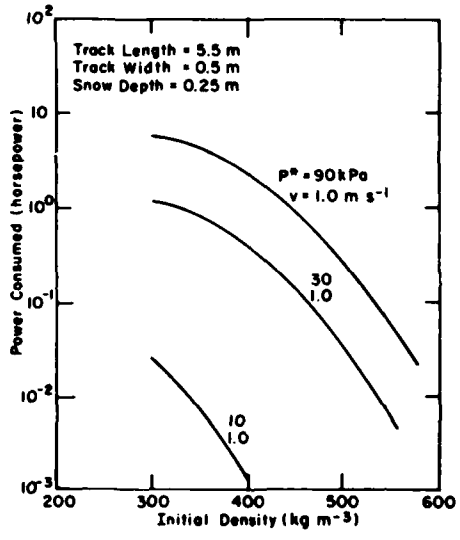

Figure 35. Effect of snow density and track pressure on power consumption in shallow snowpack.

one. The work reported here has been concerned only with the power requirement for motion through snow, which, excluding vehicle traction, is one of the most important factors affecting vehicle performance in snow.

The formulation developed here allows a detailed parametric study of the effect of several important variables on vehicle efficiency in snow. These variables include vehicle speed, track pressure, track geometry, and snowpack properties. This formulation can be useful as an analysis and design tool.

The calculations used were for snow with a uniform density and a track which develops a uniform track pressure. Such assumptions are not necessary; a stratified snowpack and nonconstant track pressure could have been used. However, the simpler problem was considered here to demonstrate the formulation.

Figure 36 shows that for the conditions assumed in our analysis, most of the energy absorbed in the snowpack is compactive. Figure 36b, on the other hand, shows that under conditions of impending slip or actual slip, it would be necessary to account for energy absorbed through shear.

The overall problem of over-snow trafficability is not fully understood and needs more work. Other sections of this report deal with problems regarding traction mechanics. One area that needs more research is the material properties of natural snowpacks. Before any detailed study of the vehicle-snowpack interaction can be made, a constitutive equation must be defined. Equation 2 accurately describes the behavior of snow subjected to loading which is predominantly a hydrostatic pressure. Currently a generalized form of eq 2 is being developed to include low density snow. However, the behavior of snow under large shearing deformations is not well understood. In particular, the effects of combined shearing loads and pressures have not been studied. Until this area is researched, it will be extremely difficult to correctly evaluate the energetics of oversnow travel for conditions of vehicle slip.

a. No-slip conditions

Figure 36. Shearing deformation in deep snowpack.

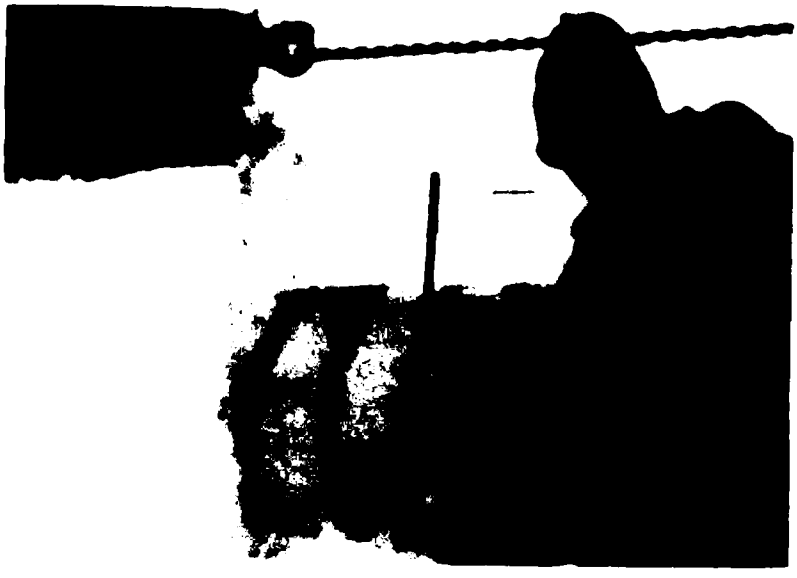

b. Severe slip conditions in drawbar pull test.

Figure 36 (cont'd). Shearing deformation in deep snowpack.

When a vehicle begins to slip, power requirements increase, as does the amount of energy absorbed in the snowpack. More work needs to be done on the energetics of this problem. Hopefully, such studies will lead to a better understanding of the effect of grouser size, design, and spacing on snowpack response and energy absorption characteristics.

References

Abele, G. and A. Gow (1975) Compressibility characteristics of undisturbed snow. U.S. Army Cold Regions Research and Engineering Laboratory (CRREL) Research Report 336, 57 pp.

Abele, G. and A. Gow (1976) Compressibility characteristics of compacted snow. CRREL Report 76-21, 47 pp.

Brown, R.L. (1978a) High rate volumetric properties of snow. (submitted for publication).

Brown, R.L. (1978b) A study of vehicle performance in snow. (submitted for publication).

Harrison, W. (1975) Vehicle performance over snow: Mathematical model validation study. CRREL Technical Report 268.

Harrison, W. (1957) Study of snow values related to vehicle performance U.S. Army Ordnance Corps LLRB Report 23.

Mellor, M. (1963) Oversnow transport. CRREL Monograph III-A4.

Yong, R.N. and M. Fukue (1978) Snow mechanics: Machine-snow interaction. Journal of Terramechanics.

PREDICTION METHODS

W.L. Harrison

Deep Snow Prediction Methods

The vane cone-McGill method and the Bekker-LLL method will be discussed and used during the field demonstration to estimate maximum drawbar pull. The required snow measurements for each method have been described in the section on snow measurements.

Vane-Cone Prediction Method. The prediction equations for the vane-cone are as follows: Maximum track traction is

$$f = \frac{\text{vane-cone torque resistance}}{\pi(\frac{d^2h}{2} + \frac{d^3}{6})} \qquad (4)$$

where d is diameter and h is height.

Vehicle motion resistance is determined by the vertical and horizontal compaction which equals

$$R = \frac{1}{L}\,(W \times Z + F \times i \times L).$$

where

W = vehicle weight

Z = dynamic sinkage

L = track contact length

i = slip at which maximum traction occurred (assumed or experimental).

The total snow resistance is defined as

$$Rt = R + Rd$$

where

Rd = f x number of tracks x 2 x grouser height.

Drawbar pull is defined as

$$DBP = F - RT.$$

Bekker-LLL Prediction Methods

The following description of the Bekker-LLL methods for predicting tracked vehicle performance in deep snow is taken from Appendix D of CRREL Technical Report 268.

Tracked Vehicle, Zero Trim Angle. It is not normal for a tracked vehicle to operate in an untrimmed attitude. The only generally accepted exception to this statement is the articulated tracked vehicle. The articulated tracked vehicle is assumed to behave as two connected units functioning as a single unit because of internal forces. The tendency of the front unit to assume a trimmed attitude counteracts the tendency of the rear unit to assume a trimmed attitude. If the rear end of the front unit sinks more than the front, the front unit will force the nose of the rear unit downward. Since the rear unit sinks more at the rear than at the front, it resists the attempt to have its nose forced downward. The forces transmitted through the articulation joint thus tend to keep the machine in a level attitude.

The amount such a vehicle will sink in a snowcover is described by

$$z = \left(\frac{p}{k}\right)^{1/n} \approx \left(\frac{W}{2b\ell k}\right)^{1/n} \qquad (10)$$

where

p = track contact pressure

W = total vehicle weight

b = track width

ℓ = track contact length

$k = kc/b + k\phi$

The snow's resistance to the motion of the vehicle is broken down into resistance due to compaction, R_c, and resistance due to bulldozing, R_b; the equations are

$$R_c = \frac{2bk(z)^{n+1}}{n+1} \qquad (11)$$

$$R_b = 2b(K_\theta z_o c + K_x \gamma z_o^2) \qquad (12)$$

where coefficients K_θ and K_x can be selected from Figure 37.

and γ = density.

The traction that the vehicle will develop is determined by

$$H = (Ac + W \tan\phi) \left\{1 - \frac{K}{i\ell} \left[1 - e^{(-i\ell)/K}\right]\right\} \qquad (13)$$

where

K = tangent modulus of the S_s vs deformation curve.

A = total contact area or $2b\ell$

i = slip value

The drawbar pull versus the weight of the vehicle (a measure of efficiency) is determined by

$$\frac{D_p}{W} = \frac{H}{W} - \frac{R_c + R_o}{W} \qquad (15)$$

A range of slip values, i, are used in eq 13 to develop the drawbar efficiency curve.

Tracked Vehicle With Positive Trim Angle. The following equations apply to the conventional tracked vehicle and are based on the assumption that the front of the track does not sink at all. Thus, there is no bulldozing resistance.

If it is assumed that sinkage increases linearly with track length, the maximum sinkage is

$$z_m = \left[\frac{p}{k} (n + 1)\right]^{1/n} \qquad (16)$$

The resistance to motion will be

$$R_c = \frac{W}{\ell} z_m \qquad (17a)$$

or, substituting for z_m from eq 16,

$$R_c = \frac{W}{\ell} \left[\frac{p}{k} (n + 1)\right]^{1/n} \qquad (17b)$$

To evaluate the tractive effort, it is necessary to obtain a numerical solution to the equation:

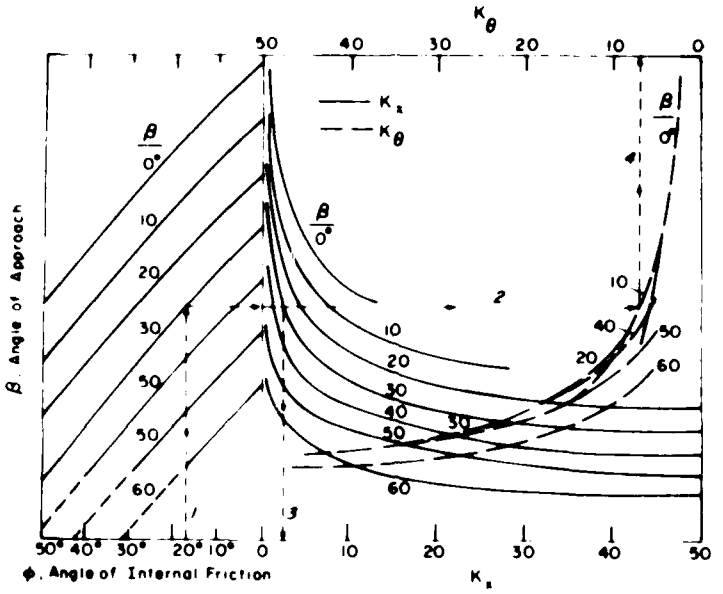

Figure 37. Chart for the computation of K_x,K_θ, coefficients of the general equation for bulldozing resistance.

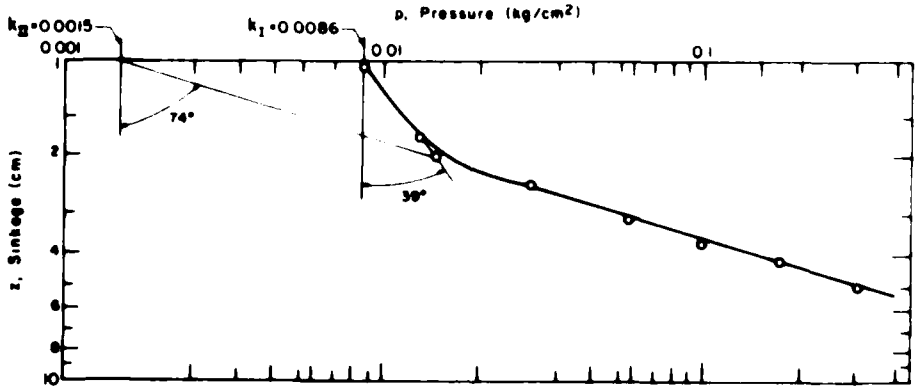

Figure 38. Pressure versus sinkage of load-sinkage function in shallow snow.

$$H=2b\ell\{c[1-\frac{K}{i\ell}(1-e^{(-i\ell)/K})]+K(z_m)^n\tan\phi\,[\frac{1}{n+1}-\frac{1}{\ell n+1}\int_0^{\ell} x^n e^{(-ix)/K}dx]\}; \quad (18)$$

where x is any length along the track/snow interface.

As before, a sufficient number of slip values, i, must be selected to permit the development of the drawbar efficiency curve.

The ratio of drawbar pull to weight is

$$\frac{DP}{W} = \frac{H}{W} - \frac{R_c}{W} \quad . \tag{19}$$

Shallow snow prediction methods

We will examine the CRREL, the Bekker-LLL, and the Army Mobility Models in this section.

The CRREL, the Bekker-LLL, and the Army Mobility Models all predict traction with the same equation:

$$H = Ac_a + W \tan \delta \tag{20}$$

where c_a and δ have been previously defined, A is the total interface contact area, and W is the vehicle weight.

The CRREL model uses the energy dissipation per unit volume, (ω) and determines the resistance with the equation:

$$R = 2b\omega h \tag{21}$$

where h is the snow depth.

Bekker proposes the following equation for determining the motion resistance of wheeled vehicles in shallow snow:

$$R = 2 (R_c + R_t) + N_w R_t \tag{22}$$

where N_w is the number of trailing wheels.
R_t is defined as the resistance due to tire flexing and reads as follows:

$$R_t = \frac{3.581\, b_o\, p_g D^2\, \epsilon(0.0349\sigma - \sin 2\sigma)}{\sigma(D - 2\delta)} \tag{23}$$

where

P_g = tire inflation pressure

D = tire diameter

ϵ = coefficient of tire wall stiffness = $1-e^{-27.5\ \delta/h}$

$$\sigma = \cos^{-1}(D - 2\delta/D) \tag{24}$$

$$\delta = (D/2) - \sqrt{(D/2)^2 - (\ell_1/2)^2} \tag{25}$$

$$\ell_1 = [W/b_o(p_g + p_c) - \ell/2F] \tag{26}$$

$$F = 1/(n + 1) \tag{27}$$

D = tire diameter

b_o = tire width

p_z = ground pressure, which is taken as the sum of inflation pressure p_g and carcass stiffness p_c

$p_z = (p_g + p_c)$.

The ground contact width, b_o, for tire load W, is determined by:

$$b_o = 2\sqrt{2r\delta - \delta^2} \tag{28}$$

where

b_o = tread width

r = tread radius

To determine resistance of the snow to motion Bekker uses a multi-layered approach based on the characteristics of plate sinkage curves in shallow snow. As shown in Figure 38, the pressure versus the sinkage is plotted in log-log curve and the "zones" are selected by observing obvious changes in slope. Each zone produces a set of k_c, $k\phi$, and n values from which the resistance for that zone can be calculated.

For "zone 1" where "n" is generally less than 3.0 or for any zone where $n < 3.0$, the resistance is determined by:

$$R_c = \frac{b_o\, k\, z_1^{(n+1)}}{n + 1} \tag{29}$$

where z_1 is determined (Bekker 1976) from the expression

$$z = \left(\frac{3W_1}{bk\sqrt{D}\,(3-n)}\right)^{\left(\frac{2}{2n+1}\right)} \tag{30}$$

where W_1 is the wheel load, defined (Bekker 1976) by

$$W_1 = 0.3\ b_o\ k\ (3-n)\ \sqrt{D}\ z_1^{(2n+1)/2} \qquad (31)$$

Whenever there is a zone where n = 3.0, Bekker states that the "full solution of the integral

$$W = b_o \int_{z_o}^{z} p_x\ d_x$$

must be used." In this function

$$W_j = b_o k_j \sqrt{D}\ [z_j^{(2nj+1)/2}\ (3_j - b_j \frac{2z_j}{D})$$

$$- z_{j-1}^{(2nj+1)/2}\ (aj - bj\ \frac{hzj-1}{D})] \qquad (32)$$

where

$$aj = (1-0.509nj + 0.222nj^2 - 0.052nj^3 + 0.005nj^4) \qquad (33)$$

$$bj = (0.25-0.26nj + 0.137\ nj^2 - 0.028nj^3) \qquad (34)$$

R_c is then the total of R_I, R_{II}.. R_j. and the total resistance wheeled vehicle is

$$R = 2(R_c + R_t) + N_w R_t \qquad (35)$$

The Army Mobility Model calculates maximum traction according to Nuttall's (1975) equation:

$$T_{max} = cA + W\mu \qquad (36)$$

where

c = interface shearing resistance (psi)

A = contact area ($in.^2$)

W = vehicle weight (lb)

μ = tangent of the angle of interface shearing resistance.

For a wheeled vehicle the mobility model calculates the ratio of resistance to weight as

$$\frac{R}{W} = (\frac{10}{n_a})\ (\frac{n_t b}{d})\ (\frac{\gamma h}{\ell}) \qquad (37)$$

where

$\ell = 2\sqrt{\delta d - \delta^2}$ (in.)

d = undeflected tire diameter (in.)

δ = tire deflection (in.)

n_a = number of axles

b = tire section width (in.)

h = snow depth (in.)

γ = snow specific gravity.

For a tracked vehicle the model defines resistance to weight as

$$\frac{R}{W} = (\frac{h}{L} - 0.15) \qquad (38)$$

where L = overall track length (in.)

The relationships were developed from a compilation of experimental test data.

Commentary

There are a number of factors worth discussing relative to the "make-up" of the equations presented. There is considerable leeway in using these models to predict vehicle performance. I am sure that the novice would be at quite a disadvantage if he tried to obtain reasonable answers to normal problems of interest. The models are very general, even though some of the equations are quite tedious.

The models depend too much on instruments that have obvious "built in" size effects to furnish snow strength parameters to apply to vehicles of different weight, size, shape, etc.

None of the equations indicate that grouser height, spacing or shape have an influence on the gross tractive effort. All models assume that the shear failure plane occurs at the grouser tips.

These are further indications that our current model is basically much too general for application to solving problems of current interest.

FIELD INVESTIGATIONS

W.L. Harrison

Two days were devoted to field investigations of vehicle traction mechanics. These studies were to evaluate current methods of predicting vehicle performance on snow-covered terrain and to allow workshop participants to observe the tests now in use.

The first day was devoted strictly to tracked vehicles in low density s w. The test site was a relatively level mountain pasture in Alta, Utah. Snowpack depth generally exceeded 2 meters. Five vehicles were provided by Thiokol Corporation of Logan, Utah, and Bombardier of Canada. These vehicles, in order of increasing weight, were the Bombi (Bombardier), the 1450 (Thiokol), the Spryte (Thiokol), the 302 (Bombardier) and the 3700 (Thiokol).

This part of the field program (1) performed drawbar pull tests to determine maximum sustained pull, (2) performed hill climb tests to find gradability of each vehicle, and (3) checked the predict methods outlined earlier by testing them against the actual performances of the five different vehicles.

Each vehicle's gradability was determined by driving the vehicle straight up a hillside of increasing grade at a preset speed (5 mph) until it was immobilized. Slope grade and sprung mass angle were measured for each vehicle. The sprung mass is the part of the vehicle that is supported by the vehicle suspension system and tends to rock back to an angle that is larger than that of the slope.

The drawbar pull tests were then conducted. A Thiokol 3700 was used as the dynamometer vehicle in all of the tests. A cable and a hydraulic load cell connected the dynamometer vehicle with the test vehicle. The test vehicle would come up to speed; then the trailing dynamometer vehicle would begin to brake until the test vehicle stopped. The load cell readings were made at the point of maximum pull before slip became noticeable and at full immobilization. The procedure was repeated four times for each vehicle, to obtain a good statistical average. During this period, the snowpack properties were measured using the Becker-LLL system and the vane cone-McGill method.

The second day of field work was involved with analysis of wheeled vehicles in dense snow cover. We tested two vehicles, the "Green Machine" owned by the Hodges Transportation Company and a similar vehicle supplied by the USDA-Forest Service Equipment Development Center. These vehicles are specially modified and instrumented to monitor wheel slip, load, and torque as well as vehicle ground speed. We measured vehicle traction in dense (packed) snow cover for a selection of tires and inflation pressures and determined the tractive capability of the tires as a function of interface velocity.

While the wheeled vehicle testing was being carried out, the rubber-faced shear annulus was used to determine c_a and δ to predict vehicle traction. The results of these predictions are reported in Appendix A.

CONCLUSIONS

W.L. Harrison, R.N. Yong, R.L. Brown

The methods and equations used in the workshop demonstrations including the minimal effort with shallow and packed snow represent many years of development and practical usage. Consultants in the field of off-road locomotion can, with their years of experience, make use of these models to assess many trends and comparisons relative to vehicles operating through and over snow. Without years of experience, the methods and equations listed herein can lead to predictions ranging from poor to irrational. As such, they cannot be classified as optimum or even ideal for application to design. One cannot assess the effects of grouser design and spacing, tire structure or tread design, to name just a few elements of design interest.

The experiment with different units for the Bekker-LLL system was done to point out the sensitivity of the method to unit length when deriving the sinkage parameters. While the traction equation can be taken as fundamental (pseudo, at least), the sinkage and resistance equations cannot.

There is always room for considerable debate and discussion as to how one chooses the correct multiple of P_n when applying the McGill vane cone (or plate) method. It is evident that the use of P_n, the nominal track pressure, for actual assessment or correlation with measured drawbar-pull values is at best naive and at worst misleading. The quandry of what to choose as an actual effective track pressure, P_e, nevertheless still remains. Whereas considerable experience in these methods will serve as guidance, much work remains to seek further clarification of the relationship between specific vehicles, P_e, and P_n.

It was concluded by the workshop participants that the current state of the art, although useful, did not satisfy the current needs. It was felt that we should be capable of predicting the effects of specific design parameters such as the structure, tread design, and track grouser design on overall performance. It was further decided that the methodology should be such that a background in engineering and/or physics should be sufficient to make intelligent application towards design and performance analyses.

Towards these ends, the following recommendations were made by the workshop participants and supported by the ISTVS Committee on Snow.

1. Base equations and methods for snow-vehicle performance predictions on fundamental laws of physics. The principles of "energetics" seem most applicable to our requirement. In many instances current models can easily be modified to meet this recommendation.

2. Consider the use of instrumented vehicles, both tracked and wheeled, for measuring strength properties of snow. Strength properties will be established to relate to shear, slip, and compaction energy dissipation. These properties will be cataloged in data bank format as probability curves relative to temperature, local environment, and other specific characteristics of the local environment.

3. Develop a generic prediction (and analysis) model which does not differentiate in the basic sense between tracks and wheels, rather than confirming two separate methodologies. This recommendation has the underlying intention of discounting popular belief that wheeled vehicles cannot operate effectively and practically in deep snow.

APPENDIX A

ANALYSIS OF VEHICLE TESTS AND PERFORMANCE PREDICTIONS

R.H. Berger, R.L. Brown, W.L. Harrison and G.S. Irwin

The snow strength measurements taken with the vane cone, plate sinkage device and shear annulus are shown in Figures A1 - A3. An analysis of the strength measurements was made by each evaluator for his part in the calculation of drawbar pull/weight performance of the test vehicles.

The documentary measurements and vehicle characteristics were as shown in the Tables A1-A4 (see text for explanation of symbols - CRREL method used).

Readers should realize that the drawbar pull measurements made during the vehicle demonstration were close estimates at best. We needed to observe the peak and ultimate loads for each vehicle. Because we used a hydraulic load cell that only recorded the peak load, an observer had to stay close enough to the test vehicles to record the sustained pull. Each vehicle was tested five times to counter possible disadvantages occurring on any single run.

Berger, Brown and Harrison computed the drawbar pull/weight ratio for each vehicle using the Bekker-LLL method. Of the three, only Harrison had experience with this method. Brown used SI units, Berger used cgs units, and Harrison used English units. Their results and comments are presented on the following pages.

Nomenclature used was as follows:

b_1 = diameter of smaller circular plate

b_2 = diameter of larger circular plate

k_c, k_ϕ, n, c, ϕ, k_x, k_θ } Bekker-LLL parameters (described in earlier presentation)

ℓ = track length at 6-in. sinkage

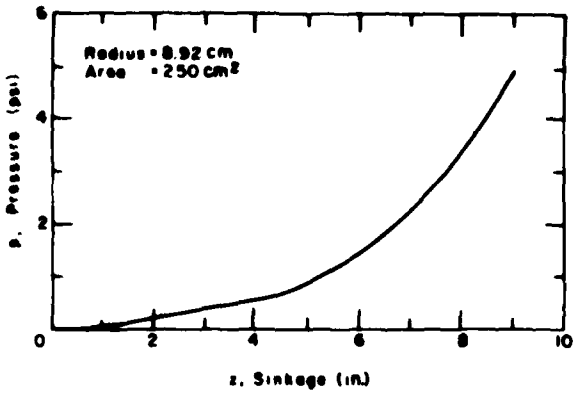

Figure A1. Pressure-sinkage curve for a 250 cm^2 plate, Albion Basin Campground.

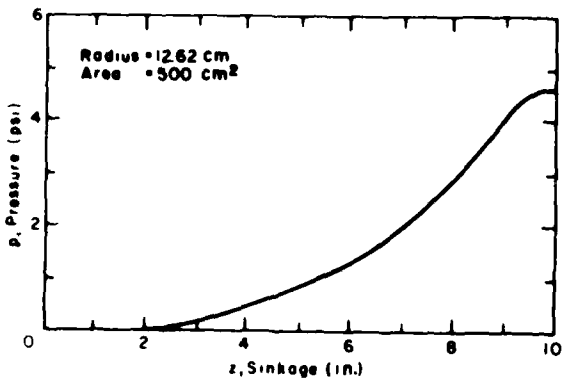

Figure A2. Pressure-sinkage curve for a 500 cm^2 plate, Albion Basin Campground.

p = track contact pressure (W/bℓ)

W = vehicle weight

β = track approach angle

R_c = compaction resistance

R_b = bulldozing resistance

H = gross tractive effort

DP = drawbar pull

The plate diameters were as indicated on the graphs. The shear annulus had the following dimensions:

inner diameter = 5.25 in.

outer diameter = 8.875 in.

Area = 40 $in.^2$

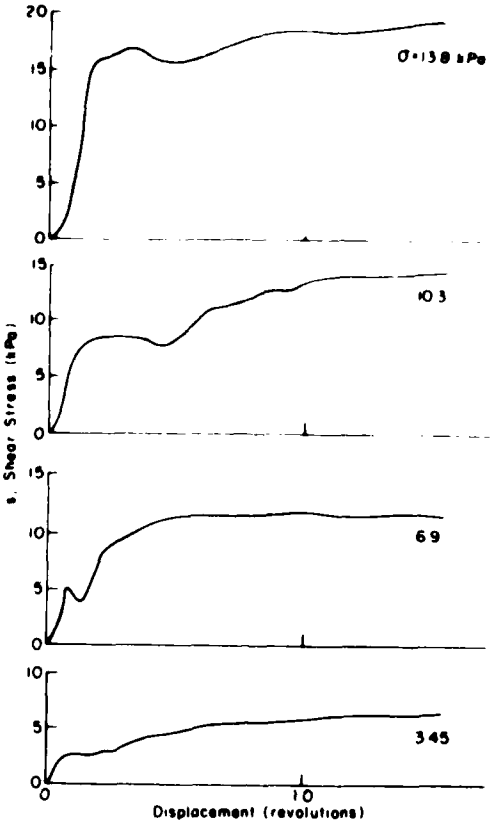

Figure A3. Shear stress-displacement curves: deep snow, Albion Basin Campground.

HARRISON

The parameters k_c, k_θ, and n were determined by a least-squares fit (logarithmic) of the following data from the load-sinkage curves:

Plate diameter 9.94 in.

Sinkage (in.)	Pressure (psi)
2	0.2
3	0.5
4	0.6
5	0.8
6	1.4
7	2.0
8	3.1
9	4.6

Plate diameter 7.02 in.

Sinkage (in.)	Pressure (psi)
2	0.3
3	0.4
4	0.6
5	0.8
6	1.7
7	2.2
8	3.3
9	5.0

The resulting values were: $a_1 = 0.08$; $a_2 = 0.058$

$k_c = 0.263$

$k_\phi = 0.005$

$n = 1.9$ (ave.)

The shear strength parameters were determined by plotting the values selected from the curves at the initial peaks that occurred during the measurement. This value was selected after considerable analysis was made as to possible instrument-induced effects. It is not typical for the shear-deformation curves to exhibit a continuous increase in strength with deformation. On the other hand, the curves are not unique as this effect has been observed in other snow tests.

A plot of the selected points as a function of the normal stress is shown in Figure A4. The resulting shear strength parameters were:

$c = 0$

$\tan \phi = 0.61$ ($\phi = 31.4°$)

$\gamma = 0.0072$ lb/in.^{3} (from Table A2)

The calculations of vehicle sinkage, snow motion resistance, and gross tractive effort are computed using eq 2, 3, 12, 15, 16 and 17.

The results of the computations are presented in Table A5 and A6.

BROWN

"Best fit" curves are calculated for the load-sinkage and shear strength-normal stress coordinates and are shown in Figures A5 and A6. Whenever curve fitting was required, a least-squares linear curve fitting routine was used to make the procedure as objective as possible. Values for k_c, k_ϕ, and n were obtained as follows:

Values of a_1 and a_2 were found by projecting the p-z curves to the $z = 1$ m intercept. Computation of k_c, k_ϕ, and n were made using these

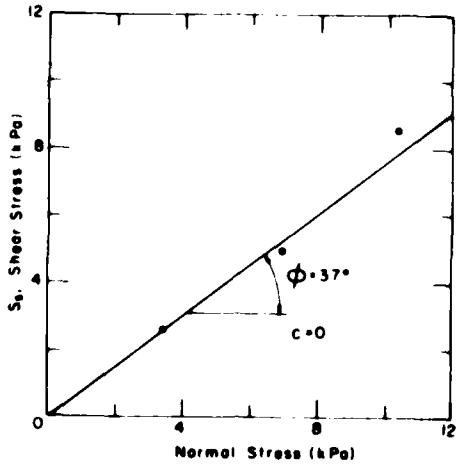

Figure A4. Plot of shear stress vs normal load (Harrison).

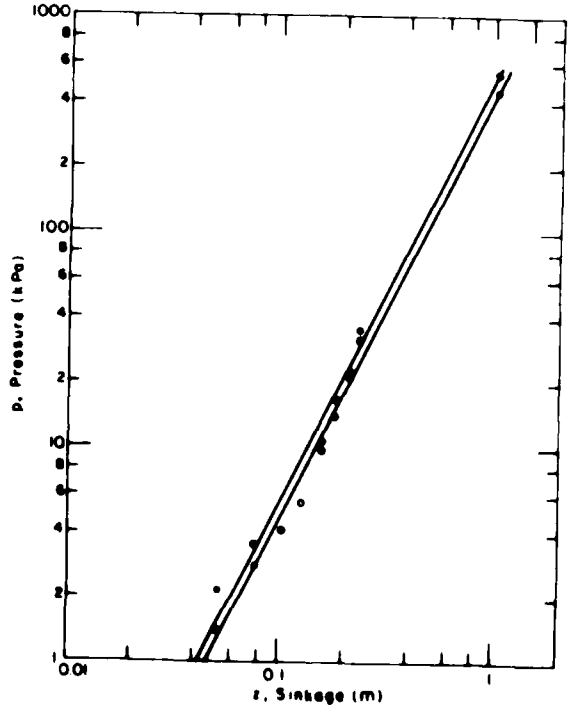

Figure A5. Log-log plot of load-sinkage curves (Brown).

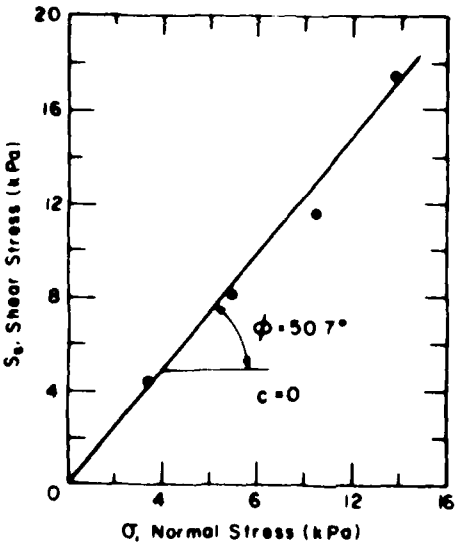

Figure A6. Plot of shear stress vs normal load (Brown).

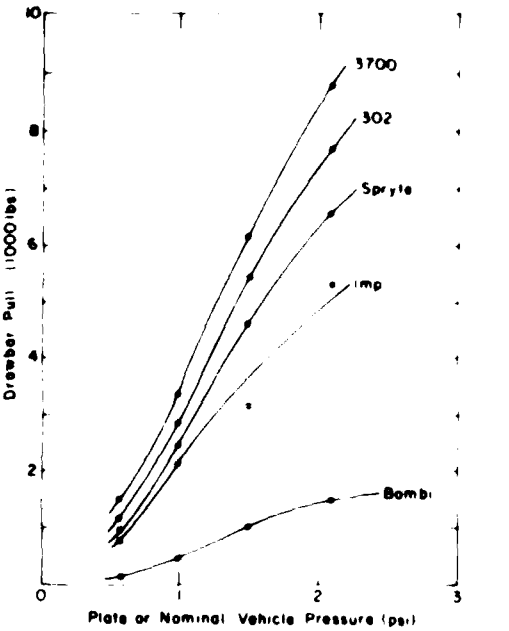

Figure A7. Plot of drawbar pull vs plate or nominal vehicle pressure.

values of a_1 and a_2, i.e.,

$a_1 = 530$ kPa

$a_2 = 450$ kPa

$b_1 = 0.0892$ m

$b_2 = 0.1262$ m

$$k_c = \frac{a_1 - a_2}{b_2 - b_1} b_1 b_2 = \frac{(530 - 450)}{0.1262 - 0.0892} (0.1262)(0.0892)$$

$$k_c = 24.34 \text{ kPa}$$

$$k_\phi = \frac{a_2 b_2 - a_1 b_1}{b_2 - b_1} = \frac{530\ (0.0892) - 450\ (0.1262)}{0.1262 - 0.0892}$$

$$k_\phi = 257 \text{ kPa}$$

$$n = \frac{\ln (110) - \ln (1.2)}{\ln (0.5) - \ln (0.05)}$$

$$n = 1.964$$

Calculations for Drawbar Pull/Weight (Summarized in Table A7)

BOMBI

$b = 0.584$ m

$\ell = 1.524$ m

$W = 11.2$ kN

$p = 6.29$ kPa

$c = 0$

$\phi = 51°$

$\gamma = 200$ kg/m^3

$\beta = 29°$

$K_x = 18.5$

$K_\theta = 75$

$$k = \frac{k_c}{b} + k_\phi = \frac{24.34}{0.584} + 257 = 298.7$$

$$z = \left[\frac{p}{k}(1+n)\right]^{\frac{1}{n}} = \left[\left(\frac{6.29}{298.7}\right)(2.96)\right]^{0.51} = 0.243 \text{ m}$$

$$R_b = [\gamma z^2 K + czK]2b$$

$$R = (1.17)(0.2)(0.243)^2(18.5)(9.8) = 2.5 \text{ kN}$$

$$R_c = \left(\frac{W}{\ell}\right) z_m K$$

$$R_c = \left(\frac{11.2}{1.524}\right) 0.243 = 1.79 \text{ kN}$$

$$H = w \tan \phi = 13.68 \text{ kN}$$

$$\frac{DP}{W} = \frac{13.68 - 2.5 - 1.79}{11.2} = 0.84$$

1450

b = 0.914 m

ℓ = 2.95 m

W = 16.1 kN

p = 2.95 kPa

c = 0

$\phi = 51°$

$\gamma = 200\ kg/m^3$

$\beta = 20°$

$K_x = 60$

K_θ = (not necessary since c = 0)

$$k = \frac{24.34}{0.914} + 257 = 284$$

$$z = \left(\frac{(3)(2.96)}{284}\right)^{0.51} = 0.171\ m$$

$$R_b = (1.828)(9.8)(0.2)(0.171)^2(60) = 6.3\ kN$$

$$R_c = \frac{(16.1)(.171)}{2.95} = 0.93\ kN$$

H = (16.1) tan 51° = 19.66 kN

DP = (19.66) - (0.93) - (6.3) = 12.43 kN

DP/W = 17.46/16.1 = 0.77

SPRYTE

b = 1.14 m

l = 3.02 m

W = 36 kN

p = 5.22 kPa

c = 0

$\phi = 51°$

$\gamma = 200\ kg/m^3$

$\beta = 45°$

$$k = \frac{24.34}{1.114} + 257 = 279$$

$$z = \left(\frac{(5.17)(2.96)}{279}\right)^{0.51} = 0.23$$

K_x = cannot be determined

K_ϕ = cannot be determined

$$R_c = \frac{(36)(0.23)}{3.02} = 2.74 \text{ kN}$$

$H = 36 \tan 51^\circ = 43.97$ kN

DP = 43.97 - 2.74 = 41.2 kN

DP/W = 1.15 (no allowance made for R_b)

302

b = 1.35 m

l = 3.0 m

W = 40 kN

p = 4.97 kPa

$$k = \frac{24.34}{1.35} + 257 = 257$$

$$z = \left(\frac{(4.97 \times 2.96)}{257}\right)^{0.51} = 0.23 \text{ m}$$

$$R_c = \frac{(40)(.23)}{3.0} = 3.07$$

$H = 40 \tan 51^\circ = 48.69$ kN

DP = 45.6 kN

DP/W = 1.14

$c = 0$

$\phi = 51^\circ$

$\gamma = 200$ kg/m^3

$\beta = 45^\circ$

K_x = cannot be determined

K_θ = cannot be determined

3700

b = 1.45 m

l = 3.05 m

W = 55.9 kN

p = 6.3 kPa

$$k = \frac{24.34}{1.45} + 257 - 274$$

$$z = \left(\frac{(6.3)(2.96)}{274}\right)^{0.51} = 0.25 \text{ m}$$

$c = 0$

$\phi = 51^\circ$

$\gamma = 200$ kg/m^3

$\beta = 45^\circ$

K_x = cannot be determined

K_θ = cannot be determined

$$R_c = \frac{(55.9)(0.25)}{3.05} = 4.65 \text{ kN}$$

$H = 55.9 (\tan 51°) = 68.2$ kN

$DP = 68.2 - 4.65 = 63.5$ kN

$$DP/W = \frac{63.5}{55.9} = 1.13$$

Comments

1. For the 302, the 3700, and the Spryte, values of K_x, K_θ, and could not be calculated from the graph. R_b was not used in calculating H and DP.
2. This system is an empirical method which is not dimensionally consistent. Therefore it works only with the English units and should not be used with either SI or cgs units.
3. A better method could be developed. For one thing, a dimensionally consistent formulation similar to the Bekker method could be developed such that it could be used in any system of units. However, this probably would still not be satisfactory, since the Bekker method does not consider the effects of track geometry and grouser design.

BERGER

Calculations (Summarized in Table A8)

$b_1 = 8.92$ cm

z(cm)	p(dynes/cm^2)	ln p = 1.92 a ln z + 1.83	$a_1 = 6.25$ dynes/cm^2
1.52	1170	$r^2 = 0.93$	$b_1 = 8.92$ cm
17.8	1660		$n_1 = 1.92$
20.3	2280		
22.9	3450		

$b_2 = 12.62$ cm

z(cm)	p(dynes/cm^2)	ln p = 19.6 lnz + 1.65	$a_2 = 5.21$ dynes/cm^2
15.2	970	$r^2 = 0.96$	$b_2 = 12.62$ cm
17.8	1380		$n_2 = 1.96$

20.3	2120
22.9	3170

$$k_c = \left(\frac{6.23 - 5.21}{12.62 - 8.92}\right) 12.62 \times 8.92 = 31.03 = k_c \text{ [dynes/cm](for a's from plot)}$$

$$k_\phi = \frac{5.21 \times (12.62 - 6.23) \times 8.92}{(12.62 - 8.92)} = 2.75 = k_\phi [\text{dynes/cm}^2]$$

The following values were used in a least-squares approximation to determine c and ϕ:

	S_s (kPa)	σ (kPa)
a)	15.20	13.80
b)	6.95	10.30
c)	6.79	6.90
d)	2.50	3.45

This resulted in values of:

$c = 0.11$ kPa $= 11$ dynes/cm^2

$\phi = 45°$

Comments

1. The units of the initial equation, $p = kz^n$, are irrational in that the units of the constant, a, have to be adjusted for each power of n; i.e. k has units [dynes/(cm)(2+n)].
2. The most subjective part of the procedure is the derivation of values from the shear plots. This leads to a large variation in the value of c, and in this case did not allow calculation of K_x and K_ϕ except for the BOMBI and 1450.

COMPARSION OF COMPUTATIONS

The comparison of computations of DP/W by Harrison, Brown, and Berger as well as the measured values are shown below. The large discrepancy in predictions is due to the selection of shear values from Figure A3 and the

computation of k_c, k_ϕ values using inches, centimeters and meters. The values under Brown shown in parentheses were computed using the value of ϕ chosen by Harrison (R_b had to be recomputed also). This was not done for the column under Berger since the results would have indicated DP/W values much lower than shown.

Test Vehicles	Harrison	Brown	Berger	Measured
BOMBI	0.50	0.84(0.47)	-1.03	0.60*
1450	0.64	0.77(0.65)	0.28	0.44
SPRYTE	0.61	1.15(0.51)	0.34	0.47
302	0.60	1.15(0.50)	0.09	0.44
3700	0.68	1.13(0.64)	-0.02	0.40

*Faulty drawbar hookup suspected: all other vehicle tests were made after correcting hookup.

The vane-cone predictions were made by Irwin. Since measurements were made in both the gradability test area and the drawbar test area (level) the results from both are presented in Tables A9 and A10. The equations described in the test under the title of "Prediction Methods" were used to calculate the values in Table A9. The calculations made in Table A9 are graphed in Figure A7 showing the predicted values of drawbar pull on level terrain for the various vehicles over a range of preloading pressures (P_n or multiples of P_n).

Table A10 shows a comparison of predicted and measured drawbar pulls on level terrain. For comparison, pull/weight ratios predicted using 1.5 P_n, 1.75 P_n, and 2 P_n are also shown.

If the nominal track pressures are used, as shown in Table A9, the predicted value, for example, of the 3700 would be a DP/W of 0.21. If, however, the effective pressure of the 3700 is in actuality 1.5 P_n the prediction as shown of 0.42 would be much more accurate. Similar assessments can be made for the other vehicles using the circled values of the P_n multiple.

There will always be considerable debate and discussion as to how one chooses a multiple of P_n. It is agreed that the use of P_n, the nominal track pressure, for actual assessment or correlation with measured DPB values is at best naive and at worst misleading. The quandry of what to

choose as an actual effective track pressure P_e nevertheless still remains. Much work remains to be done to seek further clarification of the relationship between P_e and P_n.

Table A1. Vane-cone penetrometer in undisturbed snow.

Preloading plate pressure (psi)	Plate sinkage (in.)		T^*_{max} (lb-in.)	
	from level snow	from grade	Level	Grade
0.58	3.7	4.0	1.2	2.5
1.0	5.0	5.5	3.0	5.0
1.5	7 to 7.5	7.0	5.0	8.7
2.1	8.5 to 9		7.0	

*Vane-cone torque resistance.

Table A2. Snow strength in gradability test area, 31 Jan. 1980, 14 00 hr , Albion Basin - Alta, Utah.
Wind: 3-5 mph, S.W.; Air Temp. -4°C, cloudy, light snow.

Depth (cm)	Nominal classification	Canadian hardness	Subjective hardness	Temperature (°C)	Density (kg/m^3)	Grain size (mm)	Wetness
0	new		KA	- 4		0.5	WA
20	(DB)	10	KA	- 7	296	0.5	WA
40	(DB)	40	KB	-10	296	0.5	WA
60	DB	50	KB	-11	320	0.5	WA
80	DB	95	KCS	- 5	304	0.5	WA
100	DB	50	KB	- 3	352	1.0	WA

Table A3. Snow strength in drawbar test area: 31 Jan., 1980, 1600
Albion Basin - Alta, Utah.
Wind: 3-5 mph, S.W.; Air Temp. -10°C; overcast; snowing

Depth (cm)	Nominal classification	Canadian hardness	Subjective hardness	Temperature (°C)	Density (kg/m^3)	Grain size (mm)	Wetness
0	new	01	KA	-10	--	0.5	WA
20	DB	10	KA	-14	172	0.5	WA
40	DB	30	KB	-11	242	0.5	WA
60	DB	60	KCS	-12	286	0.5	WA
80	DB	50	KB	- 8	278	0.5	WA

The vehicle parameters are listed in Table A4.

Table A4. Vehicle Parameters.

Vehicle	Track width (b) (cm) (in.)	Track length (l) (cm) (in.)	Contact pressure (p) (kPa) (psi)	GVW (W) (kg) (lb)	Sinkage (measured) (z) (cm) (in.)
BOMBI	58.42 23	152.4 60*	6.21 0.90	1134 2500	23 9
1450	91.44 36	295 116*	3.00 0.43	1633 3600	23 9
SPRYTE	114.30 45	302.26 119	5.17 0.75	3651 8050	23 9
302	135 53	300 118	5.00 0.72	4082 9000	23 9
3700	144.78 57	317.50 125	6.34 0.92	5670 12500	23 9

* Taken at 6-in. penetration (sinkage)

Table A5. Calculation of pertinent snow parameters.

Vehicle	k	z	k_x	k_θ	β
BOMBI	.016	15	10	12	29°
1450	.012	12	5.5	7	20°
SPRYTE	.011	16	23	38	45°
302	.010	17	23	38	45°
3700	.010	19	23	38	45°

Table A6. Predicted values (Harrison).

	R_c	R	H	DP	DP/W
BOMBI	625	4.96	1884	1254	0.50
1450	372	1.7	2700	2326	0.64
SPRYTE	1082	14.0	6038	4942	0.61
302	1297	15.0	6750	5438	0.68
3700	1900	19.3	9375	7456	0.60

Table A7. Summary of calculations (Brown).

	BOMBI	1450	SPRYTE	302	3700
b(m)	0.584	0.914	1.14	1.35	1.45
$\beta°$	29	20	45	45	45
ℓ(m)	1.52	2.95	3.02	3.0	3.05
W(KN)	11.2	16.1	36	40	55.9
p(KPa)	6.29	2.95	5.22	4.29	6.3
k	299	284	279	275	274
z(m)	0.24	0.17	0.23	0.23	0.25
K_x	18.5	60	----	----	----
K_θ	75	----	----	----	----
R_b(kN)	2.5	6.3	----	----	----
R_c(kN)	1.79	0.93	2.74	3.07	4.65
H(kN)	13.68	19.66	43.97	48.69	68.2
DP(kN)	9.39	12.43	41.2	45.6	63.5
DP/W	0.84	0.77	1.15	1.15	1.13

Table A8. Summary of computations (Berger).

	BOMBI	1450	302	3700	SPRYTE
Veh. Weight (W) dynes	1.11×10^9	1.60×10^9	4.00×10^9	5.56×10^9	3.58×10^9
Ground Pressure (p_2) dynes/cm	6.25×10^4	2.97×10^4	4.94×10^4	6.29×10^4	5.19×10^4
k	3.28	3.09	2.98	2.96	3.02
Sinkage z	295 cm	2-6 cm	274 cm	312 cm	279 cm
K_x	>50	22	No Intercept	No Intercept	No Intercept
K_θ	36	16	No Intercept	No Intercept	No Intercept
k_c	4.01×10^8	2.09×10^8	6.48×10^8	1.05×10^9	6.08×10^9
R_c	2.15×10^9	1.12×10^9	3.65×10^9	5.69×10^9	3.31×10^9
R_b	1.0×10^8	3.4×10^7	----	----	----
H	1.11×10^9	1.60×10^9	4.00×10^9	5.56×10^9	4.51×10^9
DP	-1.14×10^9	4.5×10^8	3.5×10^8	-1.3×10^8	1.2×10^9
DP/W	-1.03	0.28	0.09	-0.02	0.34

Table A9. Prediction of drawbar pull using vane-cone (lbf).

Preloading plate pressure (psi)	3700		SPRYTE		IMP		302		BOMBI	
	from Level	from Grade	Level	Grade	Level	Grade	Level	Grade	Level	Grade
0.58	1491	3063	977.2	2287	842	1870	1154	2688	162	492
1.0	3379	4748	2470	4742	2163	3818	2884	5566	490	1089
1.5	6200	9274	4624	8426	3148	6723	5434	9881	1016	2002
2.1	8818		6569		5312		7714		1480	

Table A10. Comparisons of vane-cone predictions for level terrain performance.

		Vane-Cone Prediction			
	Measured Pull/Weight	P_n	1.5 P_n	1.75 P_n	2 P_n
3700	0.44	0.21	0.42	0.50	0.60
SPRYTE	0.40	0.19	0.40	0.48	0.58
302	0.47	0.20	0.37	0.48	0.56
BOMBI	0.60*	0.16	0.32	0.45	0.52
1450	0.44	0.28	0.25	0.34	0.44

*Faulty drawbar hookup suspected; all other vehicle tests were made after correcting hookup.

APPENDIX B. SHALLOW SNOW TEST RESULTS

W.L. Harrison

Six test runs were made on shallow snow covering a hard surface in the vicinity of the Little Cottonwood Canyon Road Terminus. The tests were conducted with the Hodges Transportation Company's "Green Machine" and a similar (nearly identical) vehicle owned by the U.S. Forest Service Equipment Development Center. The vehicles are basically 4-wheel drive Jeep Cherokees with sophisticated instrumentation for measuring and recording forces on the traction interface and associated velocities.

Shallow snow strength properties were measured with a rubber coated annulus and are shown in Figures B1-B3.

These snow strength values (c_a and δ) were used to estimate maximum traction of the test vehicles as follows:

$$H = AC_a + W \tan\delta$$

The snow on the side of the roadway was undisturbed while the snow in the center of the roadway had been disturbed by moderate traffic.

The following values were used to estimate performance: gross vehicle weight W = 4800 lb (21.35 kN), contact area (estimated at 50 $in.^2$ per wheel) = 4x50 = 200 $in.^2$ (0.13 m^2), c_a = 3.5 kPa undisturbed and 3.2 kPa disturbed, tan δ = 0.24 undisturbed and 0.38 disturbed.

These values resulted in the following performance numbers:

Center of road: H/W = 0.40

Side of road: H/W = 0.27.

Figure B4 shows a comparison between measured values and predictions.

Since the prediction methods contain no provision for determining slip or interface velocity, only the maximum sustained pull values are shown.

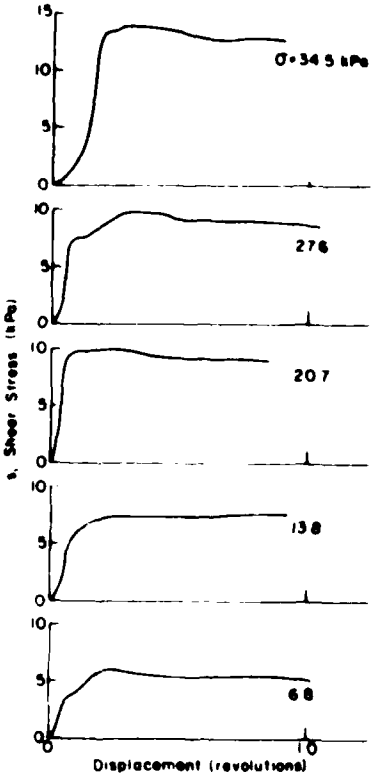

Figure B1. Shear stress-displacement curves: shallow snow; 3 cm undisturbed over packed base, Albion Basin parking lot.

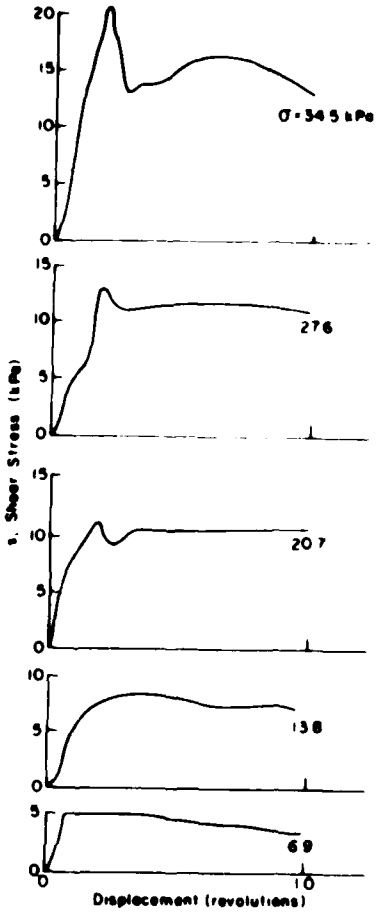

Figure B2. Shear stress-displacement curves: shallow snow; hard packed, Albion Basin parking lot.

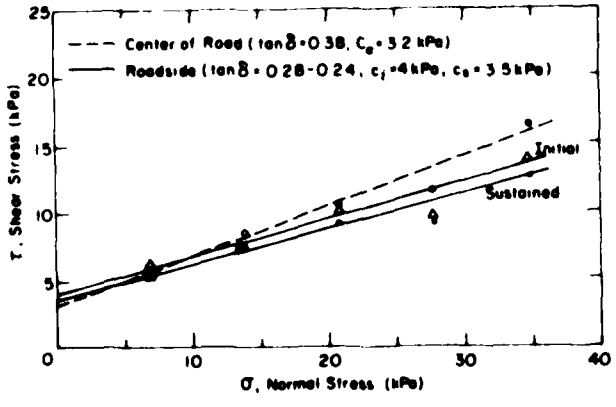

Figure B3. Shear stress vs normal load: shallow load.

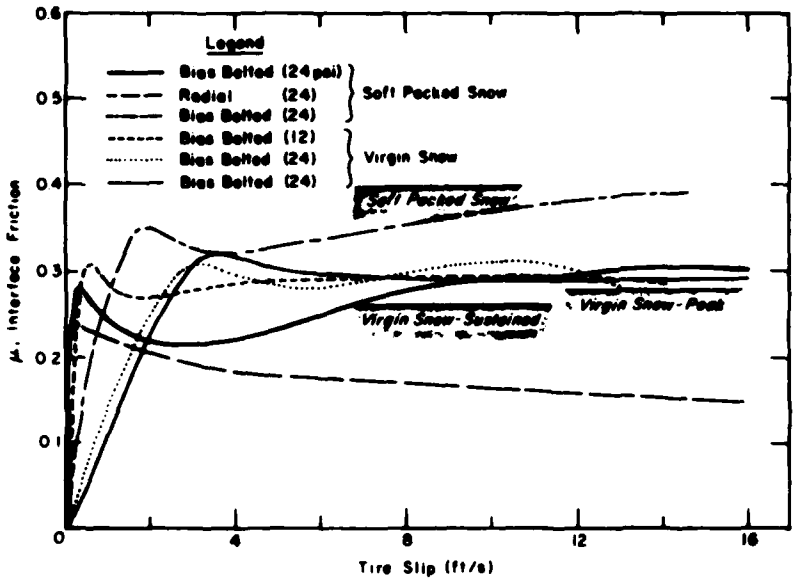

Figure B4. Comparison of experiments with predictions in shallow snow.

END

DATE
FILMED
12-81

DTIC